Energy & Buildings 300 (2023) 113624

Contents lists available at ScienceDirect

Energy & Buildings

journal homepage: www.elsevier.com/locate/enb

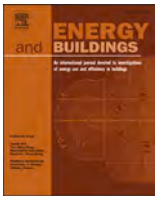

Grey-box model for model predictive control of buildings

Peter Klanatsky, François Veynandt *, Christian Heschl

Burgenland University of Applied Sciences, Campus Pinkafeld, Steinamangerstraße 21, 7423 Pinkafeld, Austria

ARTICLE INFO

Keywords:
Dynamic thermal model of building
Parameter estimation
State-space model
Resistance–capacitance model
Glass facade model
External shading model
Thermally activated building structures model
Finite difference method
Finite volume method
Data-driven predictive control

ABSTRACT

Model predictive control (MPC) can improve energy efficiency and demand-side flexibility in buildings. Developing a grey-box model suitable for MPC is not straightforward, especially in buildings combining, not only ventilation and usual internal loads, but also Thermally Activated Building Structures (TABS) and large glass façades with external shading. To address these complexities, this paper presents a reduced order grey-box approach, considering all these elements. Various single zone model structures are compared, combining resistance–capacitance model, with finite difference or finite volume methods for modelling the TABS. The performance of these various model structures is evaluated using experimental data from a well-equipped living laboratory building. Additionally, the influence of technical parameters on the model's performance is investigated.

The best model variant, with an enhanced glass façade model, achieves an accuracy of 0.25 °C of Mean Absolute Error over a year of simulation, on the 24 h zone temperature forecast compared to the measurement. This model has a small number of parameters (8), which are estimated with the least square non-linear method. The stability of the parameter values is analysed. The parameter identification requires only a small historical dataset of 1–2 weeks for startup and 2–4 weeks for training. This provides an adaptive model, in the sense that it is updated regularly (every day or week) based on recent measurement data. This data-driven evolving model is suitable across a wide range of applications involving data-driven Model Predictive Control (MPC) for buildings.

1. Introduction

Buildings account for a significant share of global primary energy demand and greenhouse gas emissions. According to the International Energy Agency, buildings are responsible for 33 % of total final energy consumption and 30 % of energy-related carbon dioxide emissions [1]. Additionally, the building sector is projected to be the largest contributor to global greenhouse gas emissions by 2050. Passive construction measures can contribute to reducing energy consumption and carbon emissions, but they may not be sufficient for a full energy transition, integrating the increasing share of variable renewables from wind and PV plants. Therefore, intelligent energy management solutions are needed to improve the demand side flexibility and the overall energy efficiency. In this perspective, a convincing strategy is Model Predictive Control (MPC) of buildings to optimise their associated Heating, Ventilation and Air Conditioning (HVAC) systems [2,3]. By leveraging data from sensors and actuators, MPC optimises heating and cooling to improve the energy efficiency and demand-side flexibility of buildings. Due to their numerical efficiency, grey-box state space models in conjunction with parameter estimators and solver-based mixed integer linear programming (MILP) methods are often used. This approach promises low engineering effort, short training periods and high scalability. However, a recent and comprehensive review highlights the remaining challenges in modelling, to achieve more mature solutions with MPC [4]. By harnessing the thermal inertia of the building mass, Thermally Activated Building Structures (TABS) are particularly interesting to gain demand side flexibility [5]. However, the large thermal inertia of TABS poses challenges for the development of appropriate modelling and control strategies [6]. Several modeling options for TABS are investigated in the present work: finite difference method, finite volume method or resistance–capacitance models.

A promising solution is to apply an MPC to TABS [5] and/or Domestic Hot Water (DHW) production. Such systems offer high energy efficiency and demand side flexibility, not only for electricity consumption (15 % savings according to [7]), but also for heating (40 % savings in [8]) and cooling loads (55 % savings in [9]). A key element of an MPC is the state space model, which enables to predict the future

* Corresponding author.
E-mail addresses: Peter.Klanatsky@fh-burgenland.at (P. Klanatsky), Francois.Veynandt@fh-burgenland.at, francois.veynandt@posteo.net (F. Veynandt), Christian.Heschl@fh-burgenland.at (C. Heschl).

https://doi.org/10.1016/j.enbuild.2023.113624
Received 21 July 2023; Received in revised form 29 September 2023; Accepted 6 October 2023
Available online 13 October 2023

Nomenclature

Fixed parameters of the zone models:

ρ_{air}	ventilation air density (kg/m^3)
$c_{p,air}$	ventilation air thermal capacity (J/kg/K)

Identified parameters of the zone models:

C_{Air}	thermal capacitance of the room air (J/K)
C_{FBH}	thermal capacitance of the heating slab (floor heating) (J/K)
C_{DE}	thermal capacitance of the cooling slab (ceiling cooling) (J/K)
C_{TABS}	thermal capacitance of the Thermally Activated Building Structures (TABS): heating or cooling slabs (J/K)
C_{ADI}	thermal capacitance of the furniture (J/K)
$1/(UA)$	thermal resistance from ambient air to room air, through the façade (K/W)
$1/h_{ADI}$	thermal resistance from furniture to room air (K/W)
$1/h_{FBH}$	thermal resistance from floor to room air (K/W)
$1/h_{DE}$	thermal resistance from ceiling to room air (K/W)
$1/h_{TABS}$	thermal resistance from the Thermally Activated Building Structures (i.e. heating or cooling slabs) to room air (K/W)
gA	attenuation coefficient of solar irradiance through the glass façade, in the simple façade model (m)
φ	correction factor of incoming solar irradiance, in the enhanced façade model (-)

Variables of the zone models:

T_{Amb}	temperature of ambient air, outside (°C)
T_{Air}	temperature of the air, in the room (°C)
$T_{Air,Measured}$	measured temperature of the air, in the room (°C)
T_{FBH}	temperature of the heating slab (floor heating) (°C)
T_{DE}	temperature of the cooling slab (ceiling cooling) (°C)
T_{TABS}	temperature of the Thermally Activated Building Structure (TABS): heating/cooling slab (°C)
T_{ADI}	temperature of furniture in the room (°C)
$T_{Vent,In}$	temperature of supply air from the mechanical ventilation (°C)
$T_{Vent,Out}$	temperature of return air to the mechanical ventilation, equals room air temperature (°C)
$\dot{Q}_{FBH}$	thermal power from heating (W)
$\dot{Q}_{DE}$	thermal power from cooling (W)
$\dot{Q}_{TABS}$	thermal power from both heating and cooling (W)
$\dot{Q}_{Solar,In}$	effective incoming solar irradiance (W)
$\dot{q}_{Solar}$	specific global solar irradiance in the glass façade plane (W/m^2)
$\dot{q}_{Solar,SF}$	specific incoming solar irradiance, after shading, with the simple façade model (W/m^2)
$\dot{Q}_{Solar,EF}$	incoming solar irradiance, after shading and glass, with the enhanced façade model (W)
$\dot{Q}_{Int,Lo}$	thermal power from internal loads: electrical power and occupants (W)
$\dot{Q}_{Vent}$	thermal power from the ventilation air flows (W)
$\dot{Q}_{Occ}$	thermal power from the occupants (W)
$\dot{V}_{Vent}$	ventilation air flow (m^3/s)
$P_{El,Tot}$	total electrical power consumption of the room (W)
c_{CO_2}	CO_2 concentration in the room (ppm)

Fixed parameters of the glass facade model:

τ_{sh}	transparency of the shading system (-)
H_{Tot}	total height of the glass façade (m)
A	glazed surface area (m^2)

Variables of the glass facade model:

$g(\Phi, \alpha, H, \gamma, f_{dir})$	attenuation coefficient of solar irradiance through the glazing as a function (-)
f_H	fraction of shaded height of the glass façade (-)
H	shaded height of the glass façade (m)
Φ	sun position: azimuth (°)
α	sun position: elevation (°)
γ	slat angle (°)
f_{dir}	fraction of direct irradiance in global solar irradiance (-)

Fixed parameters of finite volume and finite difference models, with:

subscript c	ceiling construction
subscript f	floor construction
A_r	room surface area (m^2)
x_c and x_f	thickness of each construction (m)
λ_c and λ_f	thermal conductivity of each construction (W/m/K)
ρ_c and ρ_f	density of each construction (kg/m^3)
c_c and c_f	specific heat capacity of each construction (J/kg/K)
h_c and h_f	convective heat transfer coefficient at each construction surface (W/m^2/K)
N_c and N_f	number of layers modelled in each construction (-)
N_{xc} and N_{xf}	number of elements in the thickness from the surface to the hydraulic circuit fluid (-)
N_{TABSc} and N_{TABSf}	number of elements in thickness for the thermally activated building structures (-)
$1/(h_f A_r)$ and $1/(h_c A_r)$	thermal resistance from the construction surface to the room air (K/W)

behaviour of the controlled zone over a finite time horizon. With this ability, an optimization algorithm can compute the best control action to minimize a cost function and to keep a constraint function. The cost function can consider the total energy consumption, the carbon dioxide emission, the energy costs etc. The utilization of constraint functions imposes certain technical and comfort conditions. These conditions limit the feasible solution space so that the numerical efficiency and quality can be improved.

State space models are often classified in three general categories: (1) black-box models, (2) white-box models and (3) grey-box models [10]. In short, black-box models heavily rely on data, white-box models are fully based on physical equations and grey-box models use data to calibrate simplified physical models. White-box models are not a scalable solution, because they require a lot of information and time to develop and calibrate. The black-box and grey-box models are data-driven approaches. Comparatively to grey-box models, black-box models need a large amount of historical data to achieve similar results. Recent studies show success of a black-box approach in some circumstances [11,12]. Nevertheless, most studies focus on grey-box model approaches to support a data-driven MPC strategy. Li et al. published recently the first comprehensive review on grey-box modelling for building energy simulation [13]. The challenges include theoretical limitations, confusing naming conventions, unclear model creation, and, to some extent, unknown suitable applications. The main identified applications are for control and optimisation of buildings, energy modelling at district or city level and integration of buildings in the grid. The model can represent a building part (wall, window…), a heat flux (infiltration, internal gains…), a one zone building or a multi-zone building [14], or even HVAC systems as in [15].

Developing a grey-box model for buildings requires careful consideration of several key factors such as accuracy, reliability, low computational and engineering effort, avoiding nonlinear objective and

constraint functions to support better global minimum estimation. These specifications are supported by a state space formulation based on grey box model, following the first law of thermodynamics, as a network of thermal resistances (R) and capacitances (C). They are often described as xRyC, with x the number of resistances and y the number of capacitances –y is also called the order of the model. A wide range of model structures are described in the literature from 1R1C to 8R3C, sometimes even a higher order. According to Li et al.'s review, the most common model is of second order (3R2C, followed by 2R2C) as in [7,16] and 5R1C. However, under each xRyC name, several models are possible. This depends on how the temperature nodes are connected with resistances and to which nodes the capacitances are applied. Summarising from [13]: (i) One capacitance on a temperature node between two resistances is often used to model the wall. (ii) One resistance is enough for the windows and/or the infiltrations. (iii) The thermal inertia of the interior is mostly represented either with one capacitance on the zone temperature and/or with one capacitance, connected with a resistance to the zone temperature. (iv) The heating load is often connected directly to the temperature node.

The identification of the best model depends on the building and its HVAC system, for example the heat emission system (radiators or floor heating system) [17]. For special configurations, with several zones connected through openings, a hybrid approach combining grey-box and black-box models seems promising [18]. Some recent work goes beyond the establishment of a predefined model structure, to improve the scalability of the modelling approach. [19] works on the generalisation of reduced order models, and the same team developed a framework to select a model [20]. For generalisation, several researchers use Modelica [21–23] or a Python toolbox, based on a Modelica library [24]. Even an automated data-driven modelling with machine learning seems promising [12]. Adaptive grey-box models, adjusting parameter continuously also addresses the scalability of the models [25]. In this paper, the model parameters are also updated daily with the latest measurement data.

A further way to improve the grey-box models is to account for disturbances, like measurement errors and modelling approximations, related to external and internal loads from the environment and occupants. Stochastic modelling takes these errors into account, reducing sometimes the model performance, but increasing its robustness (consistency of parameters for different training sets) [26]. Unmeasured disturbances can also be identified with a Kalman filter [27], be modelled with a resistance capacitance model [28], or even be modelled with a machine-learning-enhanced grey-box model (predictive recurrent neural network disturbance model) [29].

To calculate the solar gains, most studies use a fixed factor relatively to the measured solar irradiance [23,30,31]. When a shading system is mentioned, an ideal operation is mostly assumed [5,9] and the blind position is rarely taken into account [32]. But some studies develop specific MPC for the shading system [33,34]. As in [28], the building here under study has large glass façade, which means the solar gains play a predominant role. Handling the shading systems in the grey-box models is little present in the literature: no mention in [13].

While the studies mentioned have made significant contributions to the field of grey-box modelling in building energy systems, it's crucial to note that factors such as large glass facades, controllable shading systems, thermally activated systems, the impact of occupants, and ventilation systems have not been thoroughly examined together. Also, the combination of resistance–capacitance models with finite volume or finite difference methods for the TABS has not been found in the literature. Consequently, additional research is necessary to fully comprehend the potential of grey-box modelling in this holistic scenario. To this end, reduced-order grey-box models with short training periods and data-driven parameter estimation for such integrated system are here investigated. Various model structures are being tested and validated using measurement data from a real office building. A sensitivity analysis of the technical parameters of these algorithms is also included. The overall aim of the model development is to achieve high accuracy, broad applicability and the integrability into standardized optimization solvers.

2. Building and data used for validation

2.1. Reference building under study: Living-lab Energetikum

For the development of data-driven state space models and MPC-algorithm, a special research building has been used. The so-called *Energetikum* is a living-lab building located in a temperate climate, in Pinkafeld, Austria. It is equipped with extensive sensor technology to monitor in details the behavior of the building and its occupants. Several technologies are implemented in the building: heating, cooling, ventilation, shading, as well as energy production and storage. This offers many opportunities for experimenting and learning on these technologies.

As many buildings from the last decades, the *Energetikum* has a glass façade. Although triple glazing is used, the thermal performance of the outer wall is not as good as a well-insulated external wall construction. Most of all, the large glazing surface brings important solar loads which provide passive solar heating during winter, but can also lead to overheating in the summer months. Controlling carefully the solar loads is highly important to ensure an energy efficient operation of such buildings. The shading system consists of automated outdoor blinds, adjustable in height, with rotatable slats. The position of the blinds is monitored, so the solar gains can be deducted from measurements.

The *Energetikum* also has surface heating and cooling through hydraulic circuits in the floor and in the ceiling. A ground-source heat pump supplies the heating load, typically through the floor, and the cooling load, usually through the ceiling.

The investigated thermal zone consists of one office room of the living lab *Energetikum* (Fig. 1). This office room encompasses the most complexity - it is located in the first floor and has glass façades oriented to both south and west sides.

2.2. Dataset for testing and validation of the models

A one-year dataset is used, from January 1st 2019 to December 31st 2019, with a minutely time step. The 15 min time step data is obtained by averaging the raw variables. To generate the forecast in the first days of 2019, data from the last days of 2018 is used for the startup and training of the model.

The dataset used for this study is made available, to contribute to open science and foster further research for energy efficiency and a sustainable built environment [35].

3. Development of the grey box model structure

3.1. Overview of the model

The grey-box model developed in this task is based on an RC-model representing the dynamic thermal behaviour of a building zone. It is complemented with simple physical models of the incoming loads. The study focuses in particular on the façade model and associated solar gains, as well as on the model for floor heating and ceiling cooling. Several variants are investigated to select the best configuration.

An overview of the model structures, with all variants, is given in Fig. 2. The different variants are summed up in Table 1. The model is built with the following considerations. As the glass façade has low thermal mass, no capacitance is associated to the building envelope. Only a thermal resistance $1/(UA)$ connects the ambient temperature T_{Amb} with the room temperature T_{Air}. The internal inertia is split in one capacitance C_{Air} for the zone air –on T_{Air} temperature node– and one capacitance C_{ADI} for the construction and furniture –on T_{ADI} temperature node. The T_{Air} temperature node is associated to the measured room

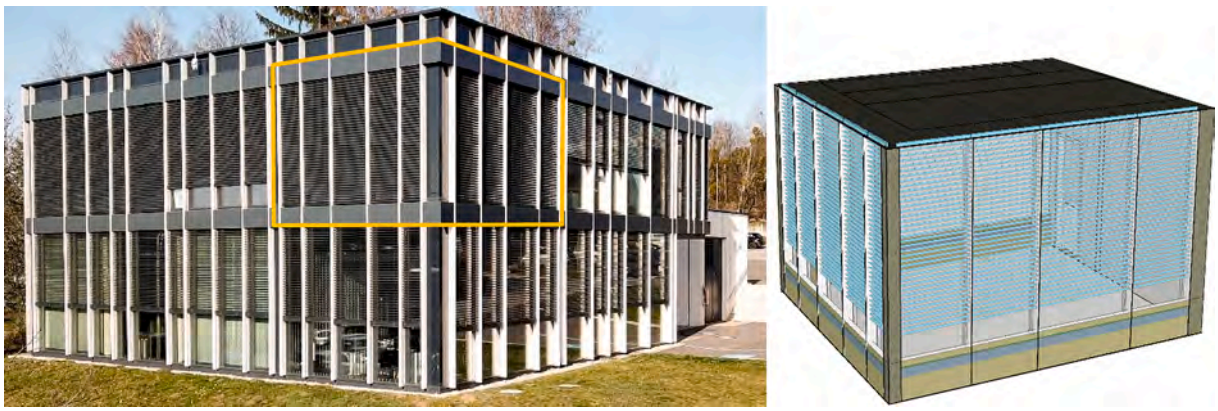

Fig. 1. Energetikum from the point of view of South-West (left) and 3D model of the office room (right).

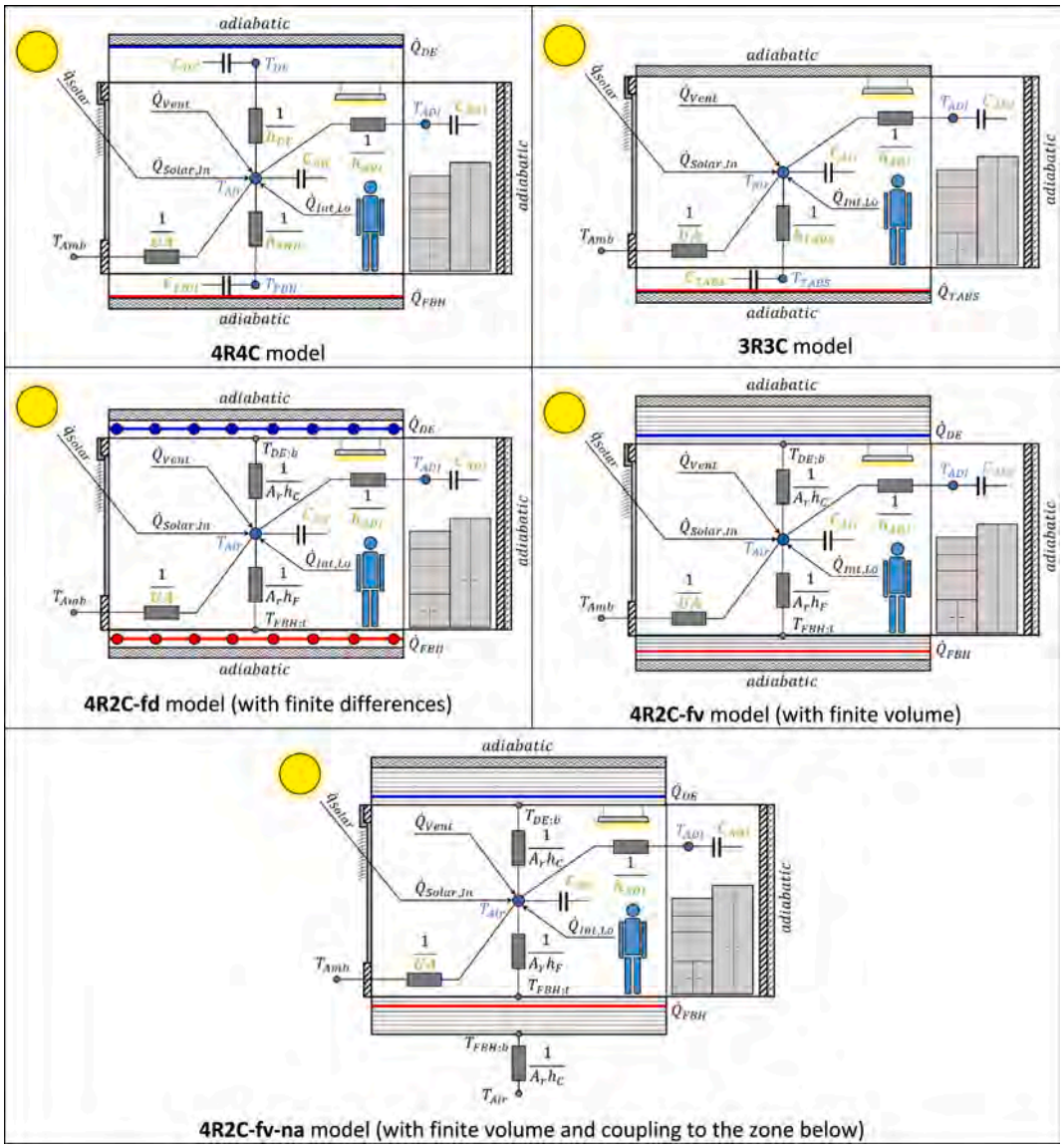

Fig. 2. Schematic representation of the investigated state space model variants. Identified parameters in **green**. (For interpretation of the references to color in this figure legend, the reader is referred to the web version of this article.)

operative temperature $T_{Air,Measured}$. T_{ADI} temperature node is considered to have no thermal losses to neighbouring rooms (ADIabatic). These two temperature nodes are connected via a thermal resistance $1/h_{ADI}$.

The variants explore four surface models for heating and cooling (section 3.2). The heating $\dot{Q}_{FBH}$ and cooling $\dot{Q}_{DE}$ loads, are applied on the T_{Air} temperature node via the thermal resistances $1/h_{FBH}$ and $1/h_{DE}$

Table 1
Overview of model variants.

Variant name	*Main specificities*
4R4C	1C on T_{Air}, 1 R to T_{amb} and 1 R to T_{ADI} with 1C on T_{ADI}. Adiabatic internal surfaces (no heat transfer to neighbouring zones). 1 R and 1C for floor heating; 1 R and 1C for ceiling cooling.
3R3C	Same as 4R4C model, but:1 single R and 1 single C for both floor heating and ceiling cooling ($\dot{Q}_{TABS} = \dot{Q}_{FBH} + \dot{Q}_{DE}$).
4R2C-fd	Same as 4R4C model, but 2 capacitances are replaced by: finite differences method for floor heating and for ceiling cooling.
4R2C-fv	Same as 4R4C model, but 2 capacitances are replaced by: finite volume method for floor heating and for ceiling cooling.
4R2C-fv-na	Same as variant 4R2C-fv model, except that the heat transfer to the zone below is considered (non adiabatic).

respectively. h_{FBH} and h_{DE} are both identified parameters. In the case of the finite volume and finite difference models, the thermal resistances between T_{Air} and the heating and cooling surfaces are $1/(h_f A_r)$ and $1/(h_c A_r)$ respectively, with A_r the room area. As the building is never heated and cooled at the same time, one model variant proposes to combine the heating and cooling loads: $\dot{Q}_{TABS} = \dot{Q}_{FBH} + \dot{Q}_{DE}$.

The solar load is noted $\dot{Q}_{Solar,In}$, calculated with a façade model, from the incoming global solar irradiance in the façade plane $\dot{q}_{Solar}$. Two façade models are proposed (section 3.3).

The influence from neighbouring rooms is considered in one variant (section 3.4), introducing the temperature node of the room air below, with the same temperature T_{Air}, connected to the ceiling temperature via the thermal resistance $1/h_{DE}$.

Other thermal loads from ventilation (section 3.5) and from the occupants (section 3.6) are also modelled. The internal load from occupants $\dot{Q}_{Int,Lo}$ and the thermal flow from the ventilation $\dot{Q}_{Vent}$ are applied on T_{Air} temperature node.

3.2. Heating and cooling loads

The building is heated up through the floor and cooled down through the ceiling. The variants explore the modelling of the floor heating and ceiling cooling hydraulic systems. In the **4R4C model** the floor heating and the ceiling cooling are modelled separately. The heat flow from the floor and the heat flow from the ceiling are each connected to T_{Air} with a resistance. The temperature nodes for heating and cooling each have a capacitance. Both temperatures are measured, corresponding to the supply temperatures of the heating, respectively cooling circuits. An expected problem of this model is the fact that the thermal inertia of the room can be represented by two free hanging parameters: the C_{ADI} and the slab that is not in use: C_{DE} during the heating season and C_{FBH} during the cooling season. This leads to an ill-posed problem, which complicates the parameter identification. Therefore, a simplified version proposes to combine the floor and ceiling equivalent resistances and capacitances.

The **3R3C** model has a single resistance and capacitance for the heating and cooling elements. With one parameter less, this model has just 8 parameters to identify. It is expected to be more robust. This model can work as heating and cooling never happen simultaneously or on the same day. If the model parameters are regularly updated, with recent seasonal data, the parameters should adjust themselves to the corresponding case of heating or cooling. In the shifting season time –spring and autumn– this approach is expected to work best if the resistances and capacitances are similar between the floor and the ceiling. A significant period without heating nor cooling or with very little loads should also be favourable to this modelling approach.

To model more precisely the heat transfer in the floor and ceiling, physical models are proposed. The **4R2C-fd** and **4R2C-fv** models are the same as the 4R4C model, except that the heating and cooling are modelled so as to account for the unsteady heat transfer in the floor and in the ceiling. In **4R2C-fd**, the heat transfer is modelled with the explicit finite differences method, while in **4R2C-fv**, the implicit finite volume method is employed. The boundary conditions for the heating and cooling power were implemented using source terms. Both numerical methods are expected to yield improved results due to their more detailed modeling of the dynamics in the thermal mass of the building. This modelling approach requires parameters to describe the construction. These parameters, summed up in Table 2, are set using data from manufacturer and building plans.

3.3. Solar gains: façade model

The heat flow from solar irradiance to the room is modelled with a specific façade model. Each of the variants presented so far are evaluated with two versions of the façade model: a *simple* façade model and an *enhanced* façade model. Fig. 3 shows schematically the enhanced façade model and the simple façade model, with their respective parameter to be identified.

The glass façade is equipped of shutters with inclinable horizontal slats. The shutters can also be set to different heights, so that the shading system can practically block from 0 to 100 % of the irradiance, depending on its settings.

In the *simple* façade model, the effective incoming solar irradiance $\dot{Q}_{Solar,In}$ (W) is calculated as:

$$\dot{Q}_{Solar,In} = gA \cdot \dot{q}_{Solar,SF}$$

with gA the identified parameter of the entire model, this is a fixed coefficient representing the attenuation (g) of the solar irradiance through the glazing over the entire glazed surface (A), and

$\dot{q}_{Solar,SF}$(W/m^2) is the solar energy that remains after crossing the shading system:

$$\dot{q}_{Solar,SF} = (\tau_{sh} \cdot f_H + (1 - f_H)) \cdot \dot{q}_{Solar}$$

with $\tau_{sh} = 15\,\%$ the fixed transparency, assumed for the shading

Table 2
Overview of parameters for the finite difference and finite volume methods.

Parameter name	Symbol	Formula, value	Symbol	Formula, value	Unit
finite difference and finite volume					
Surface of the room	A_r *Ceiling*	29.795 *surface cooling*	*Floor*	*surface heating*	m^2
Thickness of the construction	x_c	0.3	x_f	0.07	*m*
Thermal conductivity	λ_c	2.33	λ_f	1.3	W/m/K
Density	ρ_c	2400	ρ_f	2000	kg/m^3
Specific heat capacity	c_c	880	c_f	1130	J/kg/K
Convective heat transfer coefficient	h_c	10.8	h_f	$\frac{1}{\frac{1}{10.8}+\frac{0.005}{0.05}}$	W/m^2/K
finite difference					
Number of layers modelled	N_c	15	N_f	5	–
finite volume					
Number of elements in thickness from the surface to the hydraulic circuit	N_{xc}	9	N_{xf}	7	–
Number of elements in thickness for thermally activated building mass	N_{TABSc}	7	N_{TABSf}	5	–

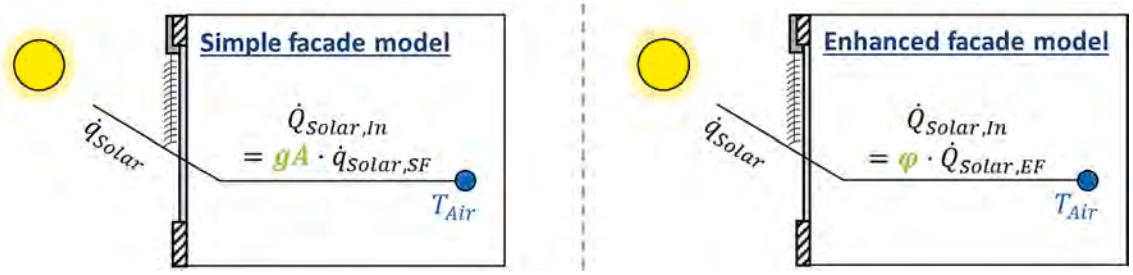

Fig. 3. Schema of the simple facade model (left) versus enhanced facade model (right). Identified parameters in **green** (gA, φ).

system,f_H the shaded fraction of glazed surface: $f_H = H/H_{Tot}$, with H the shaded height of the shutters and H_{Tot} the total height of the glass façade, and

$\dot{q}_{Solar}$(W/m^2) the incoming solar irradiance in the façade plane.

The parameter to be identified gA is an average value, which does not capture the variations of transmission with the sun position. Most importantly, the model does not represent the changes of transmittance depending on the angle of the shading slats. Therefore, an enhanced façade model has been developed.

In the *enhanced* façade model, the effective incoming solar irradiance $\dot{Q}_{Solar,In}$ (W) is calculated as:

$$\dot{Q}_{Solar,In} = \varphi \cdot \dot{Q}_{Solar,EF}$$

with φ the identified parameter, correcting

$\dot{Q}_{Solar,EF}$ the calculated solar gain, which takes into account the detailed optical behaviour of the triple glazing with horizontal rotatable slats shutter:

$$\dot{Q}_{Solar,EF} = g(\Phi, \alpha, H, \gamma, f_{dir}) \cdot A \cdot \dot{q}_{Solar}$$

with A the surface of the glazed surface, $\dot{q}_{Solar}$ the incoming solar irradiance, as already defined, and $g(\Phi, \alpha, H, \gamma, f_{dir})$ the attenuation of the irradiance through the glazing and the shading system, defined as a function of the sun position (azimuth Φ and elevation α), the shutters position (height H and slat angle γ) and the fraction of direct irradiance in the global solar irradiance (f_{dir}).

This function interpolates the information from a characteristic map, generated via a white-box model developed in IDA ICE [36]. More details are given in [37] and [38]: the first article analyses measurements to help understanding the solar gains through a triple glazing; the second article presents the characteristic map generation and the underlying white-box model. The second article shows that the enhanced façade model only slightly improves the temperature prediction. This is most probably thanks to the fact that the slat angle is always set to a value which avoids direct irradiance to enter the room through the shading. The assumption of 85 % attenuation ($\tau_{sh} = 15\,\%$) through the shutters in the simple model is therefore mostly correct. In case the slat angle is not systematically avoiding direct sun light going through, the enhanced façade model is expected to achieve much more stable results than the simple model.

3.4. Heat flows to neighbouring rooms

In the variant presented in the previous section, all internal walls, floors and ceilings and considered adiabatic. The temperature difference between the neighbouring rooms is considered small enough to neglect the thermal energy transfer to these rooms.

In one variant of the 4R2C-fv model, the **4R2C-fv-na** model, the heat transfer to the zone below is considered through a thermal resistance. This variant is expected to provide the best results, thanks to a more detailed modelling of the heat transfer for heating and cooling, including the influence from the zone below.

3.5. Heat load from ventilation

The heat flow $\dot{Q}_{Vent}$ (W) from the mechanical ventilation is modelled from the measured air flowrate $\dot{V}_{Vent}$ (m^3/s) and temperature on the supply side $T_{Vent,In}$ (°C) and the calculated room air temperature of the extracted air $T_{Vent,Out} = T_{Air}$ (°C):

$$\dot{Q}_{Vent} = \rho_{air} c_{p,air} \dot{V}_{Vent} \left(T_{Vent,In} - T_{Vent,Out}\right)$$

with $\rho_{air} = 1.12 kg/m^3$ the air density and $c_{p,air} = 1000 J/kg/K$ the specific thermal capacity of air.

3.6. Internal gains

For the heat flow $\dot{Q}_{Int,Lo}$ (W) from internal gains, the heat from the electrical power consumption is considered to 100 % and occupancy gains are estimated based on CO_2 concentration measurements: 80 W, corresponding to a resting person, is added when the concentration rises over 550 ppm.

3.7. Formulation of the model

This state space model can be formulated in matrix form, which makes the integration in an optimisation problem easy [39]. The next step is the implementation of the model in an MPC for operation of a real building. This concrete application is not presented in the present article.

4. Evaluation method

The technical parameters of the parameter identification are optimised. The physical model variants are then compared in the optimal configuration. The influence of the technical parameters has been observed on all variants. As the influence is similar on all variants, the results of the technical parameter study is presented only for the best model variant selected out of the results presented later in this article.

4.1. Test procedure for each model configuration

For each configuration, the model is calibrated and the thermal behaviour of the building zone is forecasted for the next 24 h. The procedure is schematized on a time scale in Fig. 4.

At first, the historical experimental data is used to identify the parameters of the chosen model configuration. For each day, the calibration of the model is performed at midnight. This reference time step for the start of the day is chosen to coincide with the daily updates of weather forecast and energy price, delivered at midnight. The influence of the frequency and time of day for the parameters update has not been investigated further. In the default setting, measurement data from 42 days before that reference time step are required for the startup and training of the model. The startup phase of 14 days (default) allows the model to come to a realistic state. State variables are initially set to default values, because not all are known from measurements. After the

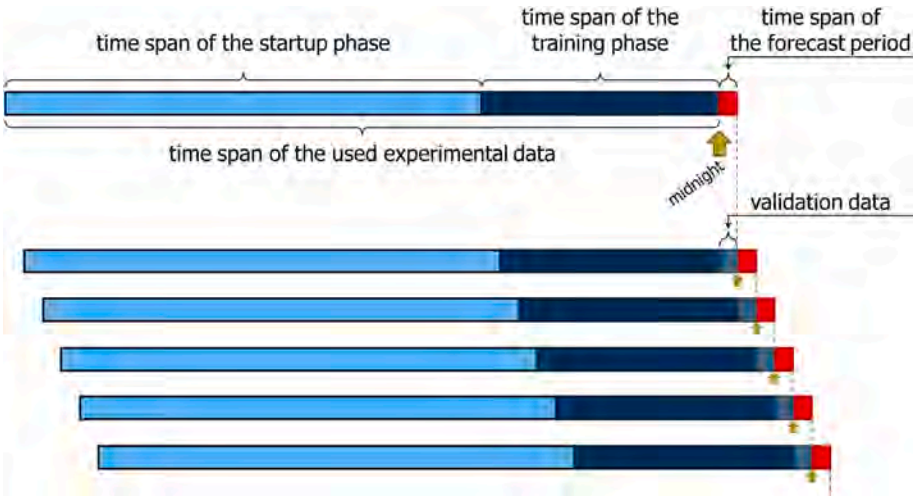

Fig. 4. Time spans of the simulation procedure (startup phase, training phase and forecast period) and respective data required. The tested time step is always midnight. The simulation is repeated for each day of the dataset.

startup, state variables have plausible values, considering the dynamics of the system. Then, the training phase starts, lasting 28 days (default). The least squares method (*lsqnonlin* algorithm in MATLAB) is used to identify the set of parameters for which the model fits best to the measurement data over this training period. The best parameter set is selected to define the model.

After that, the model runs over the prediction time span, starting from the reference time step. The thermal behaviour of the thermal zone is calculated, using: (i) the identified parameters, (ii) the real measured weather data, as an ideal weather forecast for the next 24 h and (iii) the measured internal loads (lighting, computer, ventilation, occupants) as ideal load prediction for the next 24 h. Each configuration is tested on each day of the year: 365 days from 1.1 to 31.12.2019.

The forecast for the upcoming day is compared to the measured data obtained on that same day. The smaller the deviation of the simulated room temperature to the measured one, the better the model. The aggregated results are analysed in terms of frequency distribution of the temperature deviation between the 24-hour forecast and the measurement for the same day. The Mean Absolute Error (MAE) of this deviation is calculated for the entire year. The MAE gives a physically tangible criteria, which eases the interpretation of the error. The MAE on a temperature is expressed in °C, which can be directly related to the thermal comfort. The MAE is chosen, rather than the also widely used Root Mean Square Error (RMSE). Short events outliers might be caused by an unusual situation. For example, when the sensor has been touched or a person is standing close by, abnormally high temperatures might be measured for one or a couple of time steps. Such short and rare events do not have a relevant effect on the thermal comfort in the building. Therefore, these events should not be over proportionally considered in the error evaluation. RMSE gives more importance to strong outliers (because of the square power), while MAE accounts for deviations in a proportional way [40]. This is why the MAE is preferred here, as criteria for the evaluation of the model performance. The box plot of the error distribution complements the analysis. The runtime of the entire simulation is also a key indicator for the usability of the model.

4.2. Technical parameter variation

The technical parameters for the calibration procedure are varied to investigate their influence and select an optimal configuration. The results are presented for the physical variant of the model 3R3C, with enhanced façade. This model has been selected for providing the best overall performance, according to the following analysis presented in section 5.2). The following technical parameters have been varied: simulation time step, startup phase duration, training phase duration, training algorithm, converging tolerance, maximum calls of algorithm, starting values of model parameters. The parameter values used for this study are presented in Table 3. The default parameters are indicated in bold font.

In particular, two training algorithms are tested for the parameter identification:

- *lsqnonlin*: nonlinear least square algorithm, called *lsqnonlin* in MATLAB, with the default trust-region-reflective algorithm.
- *adapted lsqnonlin*: nonlinear least square, with Levenberg-Marquardt algorithm and the option Jacobian to handle better scale problems.

The adapted parameters of the *lsqnonlin* solver have been identified as performing better in other investigations.

As for the convergence criteria, the function tolerance and the maximum number of algorithm calls are tested with two configurations: comparing 10^{-6} and 10^{-10} as set values for the tolerance, in combination with a maximum of 500 or 1000 max. calls respectively. If the algorithm does not converge below the tolerance, after the maximum number of calls, then the training stops and the best parameter set is kept.

In a perfect algorithm, the initial values of the parameter set should not influence the result. In practice, better starting values could improve the convergence stability. Therefore, two options are compared:

- *default*: fixed starting values for the parameter set or
- *previous*: the parameter set obtained in the last parameter identification (previous day) is used as starting values.

Table 3
Default technical parameters.

Parameter name	*Values investigated and unit (**default value in bold**)*
Simulation time step	1, **15 min**
Startup phase duration	7, **14**, 21 days
Training phase duration	7, 14, 21, **28**, 35 days
Training algorithm	**lsqnonlin**, adapted lsqnonlin
Converging tolerance Maximum calls of algorithm	$\begin{Bmatrix} 10^{-6} \\ 500 \end{Bmatrix}$, $\begin{Bmatrix} 10^{-10} \\ 1000 \end{Bmatrix}$
Starting values of model parameters	**Default values**, Previous values

5. Results from model training and validation with experimental data

5.1. Technical parameters variation analysis

Table 4 shows a selection of variants, investigating technical parameters, with their respective Mean Absolute Error (MAE) and the run time. It should be noted that the runtime is relevant in terms of order of magnitude: for any given configuration, simulation time variations in the range of 20 % have been observed on the same computer.

The error distribution of the indoor temperature evaluation for each variant is also presented in a box plot in Fig. 5. The middle line in the box is the median value and the box contains 50 % of the points. The whiskers are at most 1.5 times longer than the box, which leads to 0.7 % of outliers if the distribution is normal. The percentage of outliers is indicated in the diagram. With over 2.3 % in all cases, the distribution is more spread out than the normal distribution.

5.1.1. Simulation time step

The influence of the simulation time step is tested with 1 min (variant *Ref.*) and 15 min (variant *Step*) time step duration. The building does not have a strong thermal inertia, which results in a temperature variation over time of up to 1 °C per hour. In most of the cases, the strongest daily temperature variation over time is in the range of 0.5 °C per hour or below, as illustrates Fig. 6 on an autumn day.

From this perspective, a 1-minute time step is superfluous. A 15-minutes time step is enough to capture correctly the dynamics of the temperature variations in the building. In general, averaging over 15 values, as in the coarser resolution, tends to lead to lower MAE. Similar results quality are actually obtained by both variants, achieving 0.25 °C of MAE. Short term effects –like opening a window– are not modelled correctly and might be visible in the minutely measurements. This can explain the slightly wider spread of outliers with the 1-min time step, as observed in Fig. 5. These short-term variations are not critical for the energy balance of the building over the day. A clear advantage of the 15 min time step is on the runtime: the simulation takes 6 min with the 15-minutes time step, while the shorter time step requires an over-proportionally longer runtime exceeding two hours.

5.1.2. Startup phase duration

The startup phase durations of 7, 14 and 21 days are tested respectively in variants *Stt7*, *Ref* and *Stt21*. After the startup, a 28 days-long training period begins.

With 7 days startup, the results are already satisfying with 0.26 °C MAE. Nevertheless, 14 days training further increases the stability of the model, with slightly smaller error bars on the boxplot of Fig. 5. 14 days startup improves the MAE by 5 % for a non-significant increase of the runtime (14 %). Extending the startup phase to 21 days neither improves the MAE, nor reduces the error bars. The runtime is also 24 % longer than the reference. Therefore, the 14 days startup phase duration is selected.

5.1.3. Training duration

After the startup phase of 14 days, the training phase starts. The training times of 7, 14, 21, 28 and 35 days are tested respectively in variants *Trn7, Trn14*, *Trn21, Ref* and *Trn35*.

Interestingly, a shorter training phase yields lower MAE of down to 0.22 °C with just 7 days training. The drawback is an increased number of outliers as the boxplot in Fig. 5 shows. This is a sign of reduced reliability of the model: it performs in general well, but some days happen to be significantly worse. These failing cases might well be related to the switch between operation modes: active heating, active cooling or free running, when the building is neither actively heated nor actively cooled. In the 3R3C model structure, the parameters h_{TABS} and C_{TABS} play a different function in each of these modes, respectively representing: the heating load, the cooling load and the inner thermal inertia, like h_{ADI} and C_{ADI}. It could be observed that the longer period without heating or cooling in the present dataset does not exceed 11 days. This might explain why 14 days or longer training durations show significantly less outliers than in the 7 days training duration case. This also contradicts the hypothesis that longer free running periods are beneficial for the 3R3C model stability, when switching between heating and cooling operation modes.

For a deeper analysis, the diagrams in Fig. 7 show the timeline of temperature forecast for the various training durations on three months of the year. Similar performances of the models are generally observed. At the start of the cooling period in June, all models react similarly good. At the start of the heating period in November, 7 and 14 days training lead to several days with a higher error in the order of 1 °C. The 21 and 35 days training variants also have several days with deviations of up to 0.5 °C. Here the 28 days training model (Ref.) performs best. In September and June, the model with 35 days training shows also more days with higher deviations at the daily extrema. The 11 days of free-running operation occur at the beginning of the heating period. With just 7 or 14 days, the model has no to very little data with active heating or cooling. This seems to confirm the source of the failure with the shorter training periods. The duration of free-running operation should be kept in mind, when using the 3R3C model, with combined parameters for heating and cooling.

From the overall analysis, 14 days is the minimum period that ensures a reliable training. A training period longer than one month (35 days) tends to reduce the results quality, with wider error bars. The identified optimum training duration lies between 14 and 28 days. The simulation runtime varies linearly with this parameter, from 300 to 380 s for the optimal range. The longer training period of 28 days is selected for the rest of the study. Alternatively, to save computing efforts, 14 days should also be enough.

5.1.4. Training algorithm

The *lsqnonlin* algorithm (variant *Ref.*) is compared to the *adapted*

Table 4
Parameter variation of technical parameters. Color scale: best | average | worst

Variant name		Ref	Step	Stt7	Stt21	Trn7	Trn14	Trn21	Trn35	Algo	Conv	Initial
Model		3R3C										
Façade model		enhanced										
Time step (min)		15	1									
Phase duration	Startup	14		7	21							
	Training	28				7	14	21	35			
Training algorithm		lsqnonlin								adapted		
Converging tolerance Max. calls of algorithm		$\{10^{-10}$ $1000\}$									$\{10^{-6}$ $500\}$	
Parameters initial values		default										previous
Results	MAE (°C)	0.250	0.248	0.263	0.252	0.223	0.243	0.244	0.274	0.348	0.252	0.253
	Runtime (s)	382	7473	334	475	234	299	345	466	590	215	346

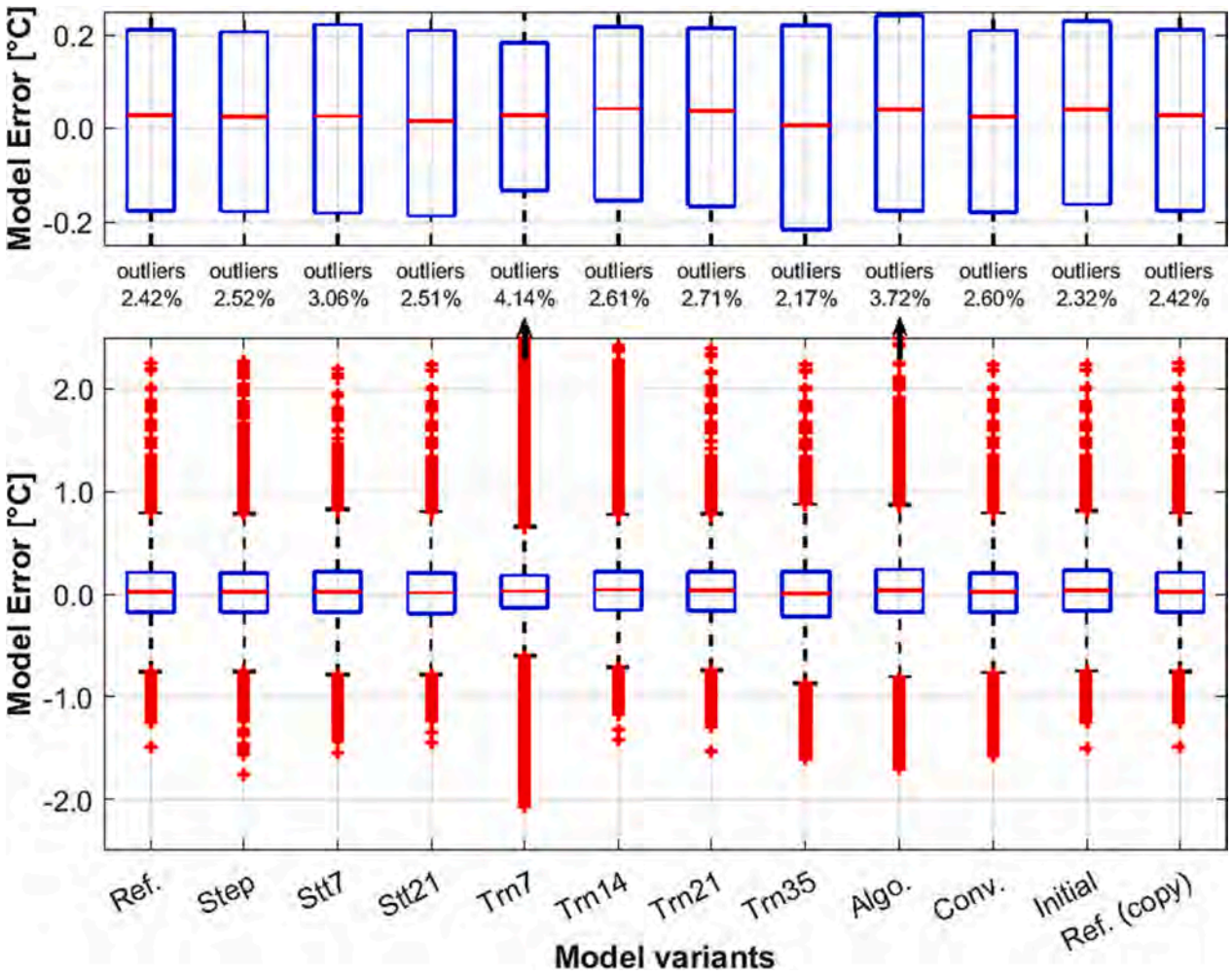

Fig. 5. Box plots of error distribution on indoor temperature forecast for the selected model variants: zoom on the quartiles box (top) and overall view with outliers (bottom). The arrows indicate there are some more outliers outside of the plot limits.

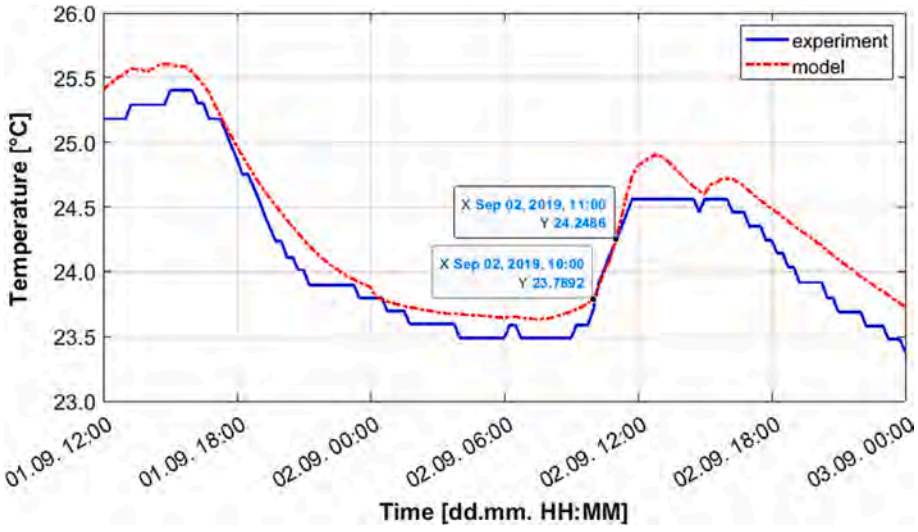

Fig. 6. Example of temperature variation over time in the room: close to 0.5 °C in one hour.

lsqnonlin (variant *Algo.*). The tests here do not reveal any improvement with the *adapted lsqnonlin*. On the contrary, the *adapted lsqnonlin* takes 50 % longer and the MAE obtained is 39 % higher than with the default *lsqnonlin* solver. The degraded performance is explained by the occurrence of a day when the model does not converge, as Fig. 8 shows.

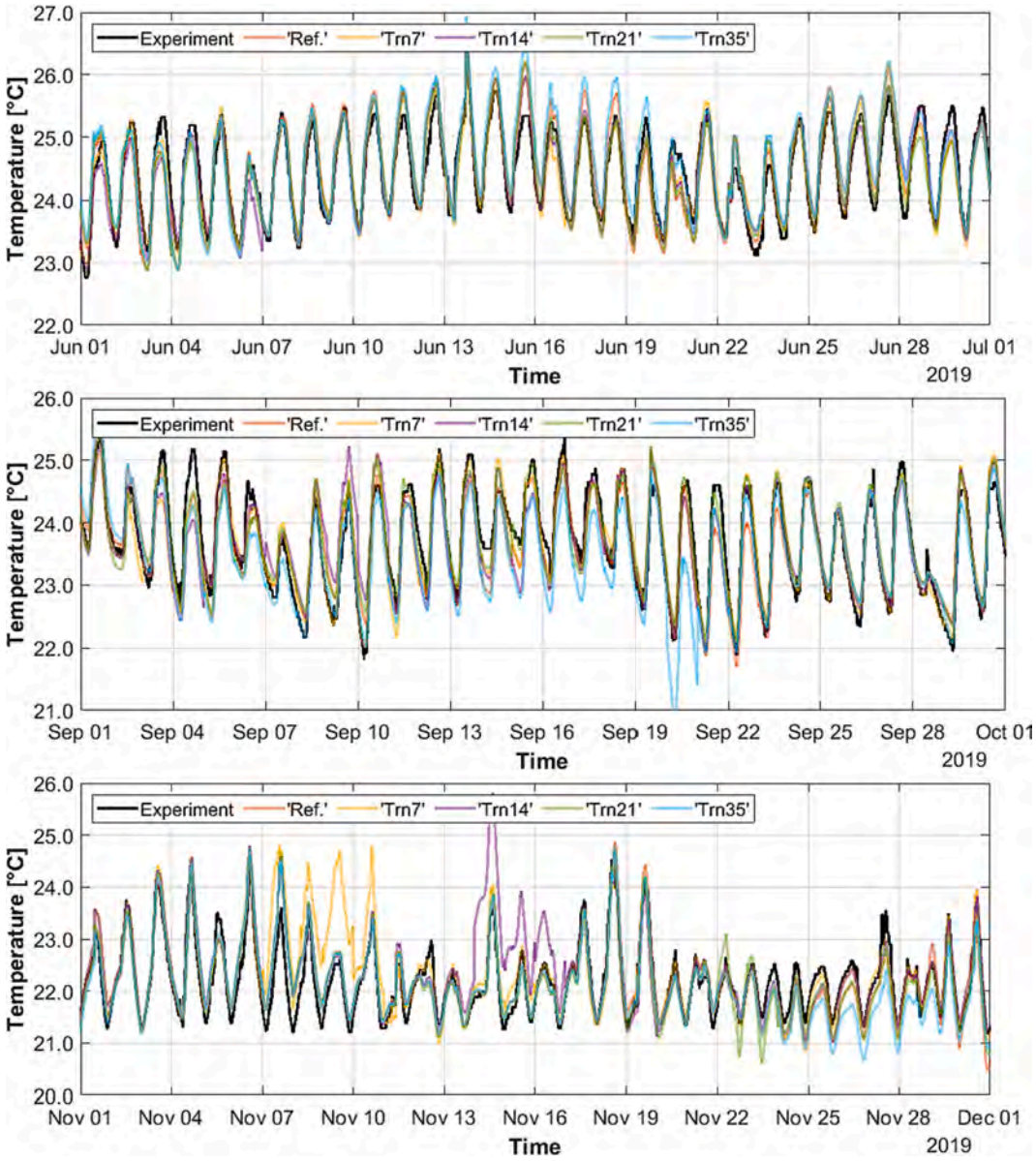

Fig. 7. Monthly timeline of temperature in the building zone: comparison of measured (Experiment) and forecasted with different models, varying the training time: 7, 14, 21, 28 (Ref.) and 35 days. Top: June (start of cooling period), Middle: September (intermediate season) and Bottom: November (start of heating period).

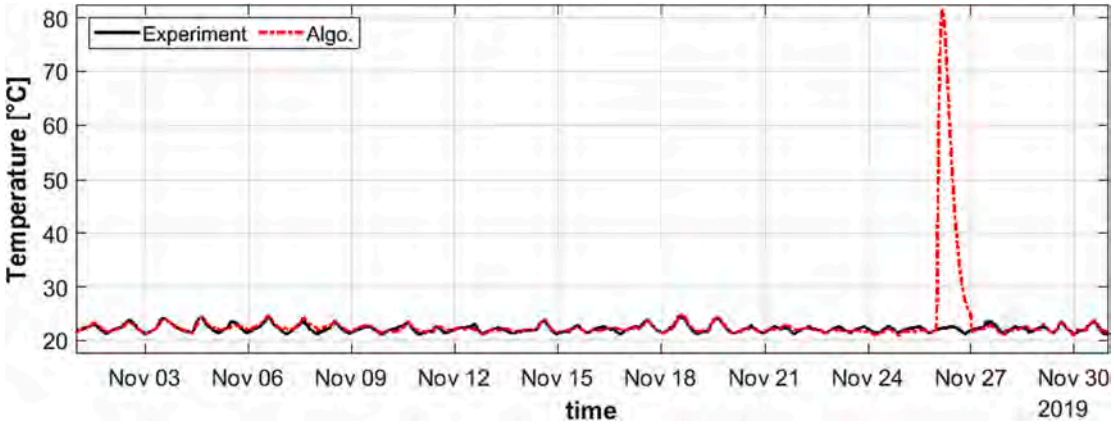

Fig. 8. Comparison of measured (experiment) and forecasted (model) temperature profiles (°C): visualisation of abnormally high temperature forecast error on November 26th 2019, because of failed parameter identification (unique occurrence over the tested year) in the *Algo* variant, using the *adapted lsqnonlin* solver.

5.1.5. Converging tolerance of the training algorithm and maximum calls of the training algorithm

The two tested configurations of the convergence criteria –fine as in Ref. and coarse as in Conv.– have little influence on the results quality. The runtime of the coarse convergence parameters is 44 % shorter than the fine parameters. Nevertheless, in some configurations, the coarser convergence criteria lead to some instability. This has been observed for model 4R4C with enhanced façade and 15 min time step, as well as for model 3R3C with simple façade and 1 min time step. In these cases, on rare days, no convergence occurs before the maximum function calls number of 500 is reached. This failed parameter identification causes abnormally high errors in the temperature forecast, with simulated values up to 13 °C far away from the expected state of the building.

Additional variants of the convergence criteria are introduced here to investigate further the cause of these failure. While keeping the coarse convergence tolerance at 10^{-6}, the maximum number of function calls is varied: 500 for *coarse*, 1000 for *coarseA* and 2000 for *coarseB*. In Fig. 9, the error distribution of selected configurations is shown in box plots. The effect of the failed identification with the *coarse* criteria can be seen in the increased number of outliers in the yearly statistics. In these cases, increasing the maximum number of function calls to 1000 solves the problem (*coarseA*). Increasing it further to 2000 (*coarseB*) does not bring any difference. In model configurations without failing convergence, the finer converging criteria show only marginal improvement in the quality of the parameter identification process.

Fig. 10 shows the distribution of number of function calls at convergence for the failing configurations. In the *4R4C-EF-15* min-*coarse* configuration, the maximum number of calls is reached in almost half of the cases (48 %). In *3R3C-SF-1* min-*coarse* this occurs in less than 4 % of the cases. Fig. 11 shows the same plots for the *Ref.* and *Conv.* models. The distribution falls nearly to zero with a greater distance from the maximum. Still, the plots reveal that the *Ref.* model reaches the maximum in 1.5 % of the cases and the *Conv.* model in 0.2 % of the cases. The share of cases when the maximum is reached is not a criteria to avoid bad parameter sets for the model. Nevertheless, this should not happen too often to reduce the probability of high error in the identified model.

For this study, the finer convergence criteria are chosen despite the increased runtime, to ensure higher stability. For runtime optimisation, the combination of 10^{-6} of convergence tolerance and 1000 maximum function calls (*coarseA* criteria) is advised.

5.1.6. Starting values for the parameter set

The variant *Initial* uses the *previous* parameter set as initial values for the parameter identification. This leads to similar results quality with 0.253 °C of MAE, instead of 0.250 °C with the *Ref.* variant, using fixed *default* initial values for the parameters. The runtime of the variant using *previous* values is also 10 % shorter. The default values can be used securely in the following study.

5.1.7. Discussion on the scalability of the technical parameter study

The reference set of technical parameters selected is used in the analysis of the different physical model variants, which is presented in the next section. It should be noted that the optimal set of parameters might vary if the method is applied to other buildings. This is the object of the discussion here.

The thermal inertia of the building is expected to affect the minimal time step that should be used in the building. The present building is a rather light construction with fully glazed facades. The ceiling and floor alone, together with the furniture, build up the thermal mass of the building. The time step of 15 min is therefore adequate for most buildings, with at least as much thermal inertia.

The startup phase duration fixed at 14 days is also expected to be affected by the thermal mass of the construction. The heavier the construction, the longer the startup phase. A duration of 14 days should also be suitable for somewhat heavier construction than the one of *Energetikum*.

The training phase seems clearly to need more than one week. One reason is probably the climate which is often varying every 5 to 10 days. A two week period will often have various climate conditions to train the model for all possible weathers. The model also reveals to have certain seasonal variation. A training period of more than one month is not as good to predict the next day as a shorter period. A complementary test has been performed by running yearly forecast simulations with fixed parameter values –taken from the daily parameter identifications. This test confirms that any fixed parameter set does not perform well all year round. This validates the strategy of repeating daily the parameter identification. To save further computing resources or for larger

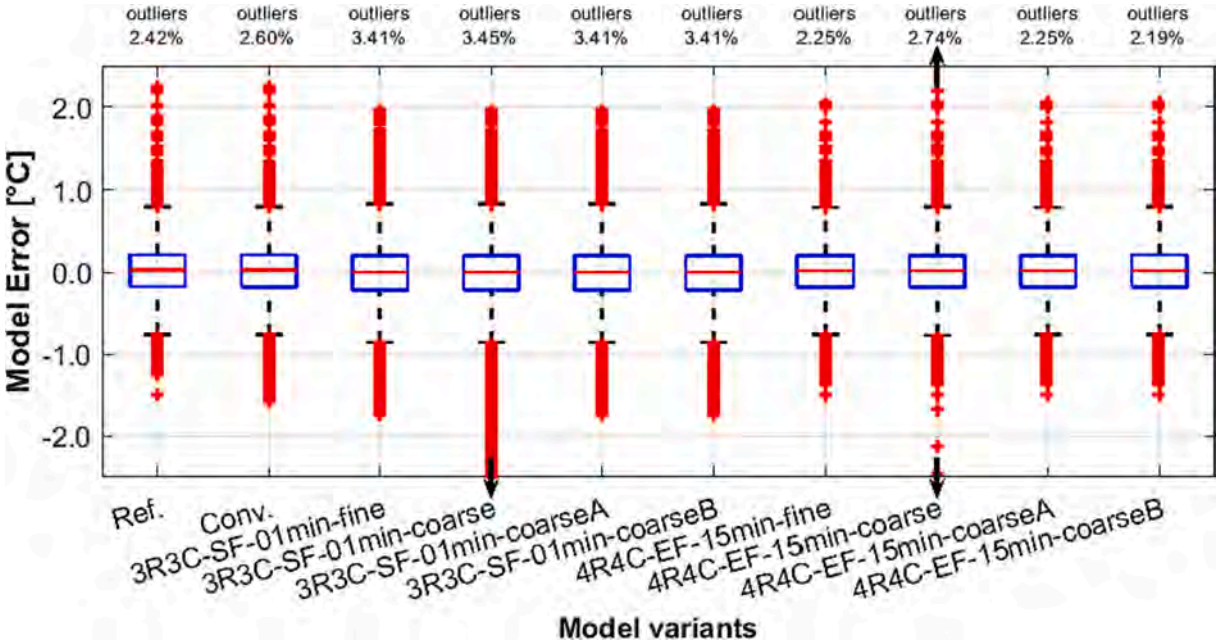

Fig. 9. Box plot of selected configurations with different convergence criteria: *fine* (as in *Ref.*: 10^{-10} tolerance, 1000 max. function calls), *coarse* (as in *Conv.*:10^{-6} tolerance, 500 max. calls), as well as *coarseA* (10^{-6} tolerance, 1000 max. calls) and *coarseB* (10^{-6} tolerance, 2000 max. calls).

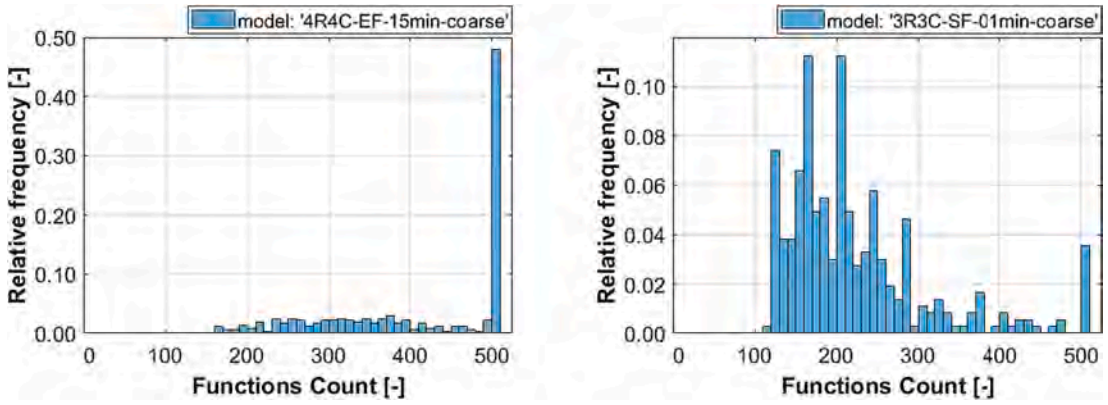

Fig. 10. Distribution of number of function calls at convergence for the failing configurations.

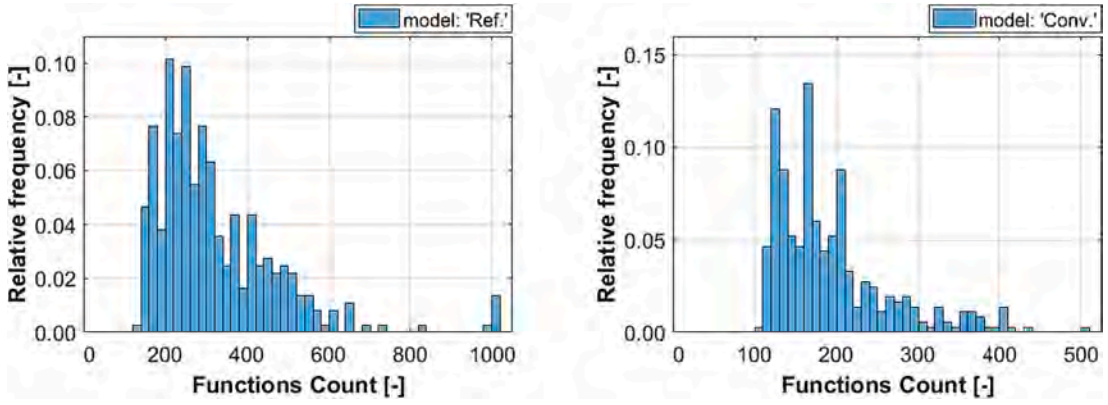

Fig. 11. Relative frequency distribution of number of function calls at convergence for the Ref. (fine convergence criteria: 10^{-10} tolerance, max. 1000 calls) and Conv. (coarse convergence criteria: 10^{-6} tolerance, max. 500 calls) configurations.

buildings, weekly parameter identification should still give good results.

The present solver proves robust. It can probably be applied for other buildings. The convergence criteria should also remain valid as long as the number of parameters to identify remains the same. If convergence problems occur, adjustment of these parameters should provide a solution.

The fixed initial values for the parameter identification provide the same results than using previous values and can be used with confidence.

5.2. Physical model variants study

5.2.1. Overview of results

The model variants 4R4C, 3R3C, 4R2C-fd, 4R2C-fv and 4R2C-fv-na, as defined in Table 1, are compared in the following. The results of the physical variants, including the façade variants, are presented in Table 5 and Fig. 12. The results for the simple and enhanced façade models are similar on all variants. For clarity, the results of the simple façade model are presented only for model 3R3C. The results for the finite difference model (*4R2C-fd*) are presented for 1 min time step, because no results can be obtained with the 15 min time step: time step too long compared to the dynamics in one discretised layer.

5.2.2. Frequency distribution of temperature forecast deviation with 3R3C and 4R4C models with both façade models

Fig. 13 shows the frequency distribution of the temperature deviation between forecast and measurement, for the models *3R3C* and *4R4C*, with the two façade model variants. These diagrams complement the information from the boxplots by showing the shape of the distribution, truncated at ±1 °C error. The distribution comes closer to a bell shape with the enhanced façade model, but all look very similar and regular.

5.2.3. Temperature timeline with 3R3C model with enhanced façade

The variant 3R3C with enhanced façade model achieves the lowest MAE: 0.247 °C. It corresponds to a temperature forecast deviation below 0.4 °C in 80 % of the time steps. Fig. 14 gives an overview of the forecasted temperature profile in the building zone, compared to the measured one over the entire year. Fig. 14 also zooms on two weeks of the same profile. It is noticeable that some days perform outstandingly, while some others have deviations in the order of 0.5 °C but rarely up to

Table 5
Physical variants. Color scale: best | average | worst

Variant name		*3R3C-SF*	***3R3C***	*4R4C*	*4R2C-fd-1min**	*4R2C-fv*	*4R2C-fv-na*
Model		*3R3C*	*3R3C*	*4R4C*	*4R2C-fd*	*4R2C-fv*	*4R2C-fv-na*
Façade model		*simple*	*enhanced*	*enhanced*	*enhanced*	*enhanced*	*enhanced*
Results	*MAE (°C)*	0.2747	0.2500	0.2473	0.4615	0.5158	0.6992
	Runtime (s)	407	382	1215	19536	4614	8452

*: results for 1 min time step, instead of 15 min elsewhere, because simulation fails in this case.

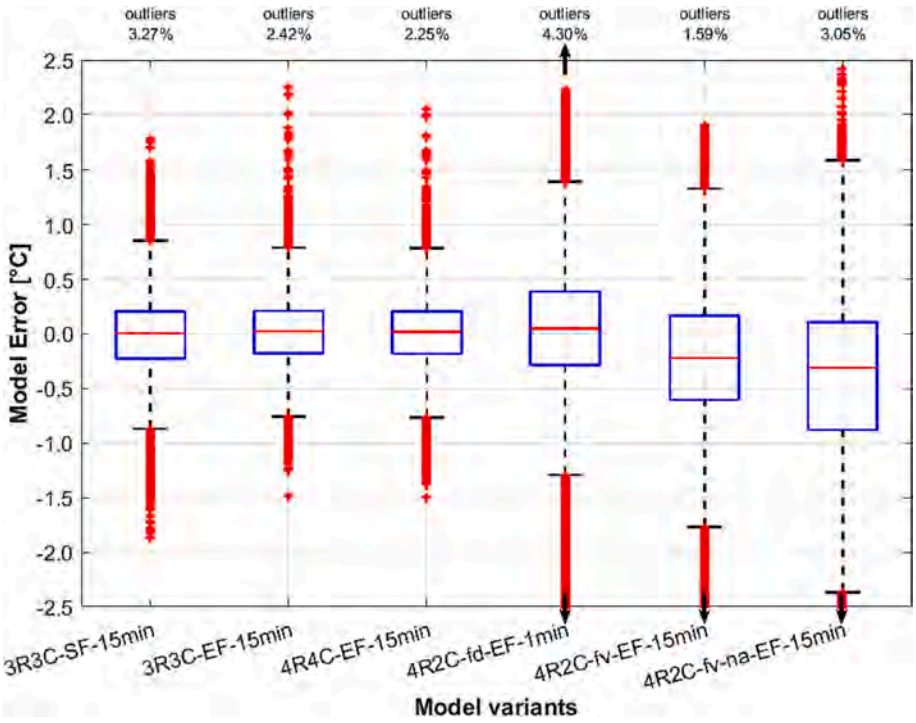

Fig. 12. Box plots of the physical model variants. Note: 4R2C-fd-EF is with 1 min time step, instead of 15 min for all other variants.

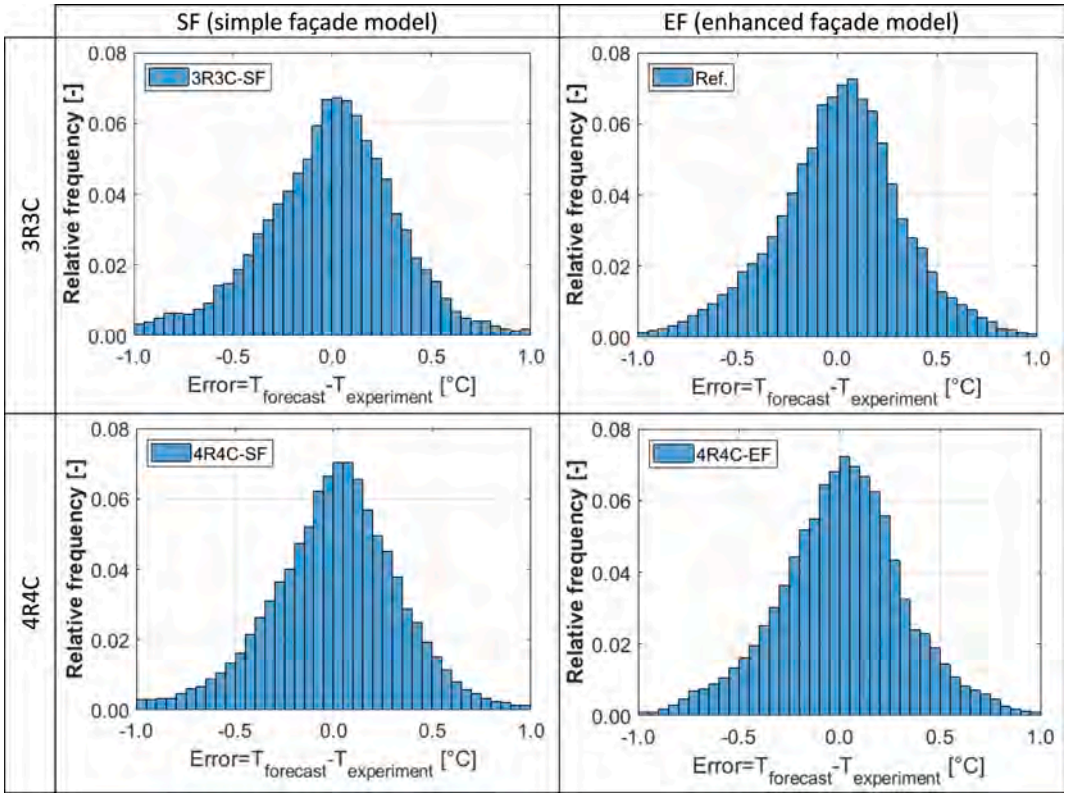

Fig. 13. Relative frequency distribution of the temperature deviation between the 24-hour forecast and the corresponding experimental data, for the 3R3C model (top) and 4R4C model (bottom) in two façade model variants: simple (left) and enhanced (right).

1 °C, as the statistics confirm (MAE, boxplots).

5.2.4. *Discussion of the RC model structure*

Unexpectedly, the models with the *finite differences* (*4R2C-fd*) and with the *finite volume* (*4R2C-fv*) do not provide better results (with either of the façade models). As the box plots in Fig. 12 show, the *4R4C model* and *3R3C model* give significantly better results with 40 % smaller error bars on temperature forecasts. The *4R2C-fd* variant, requiring 1 min

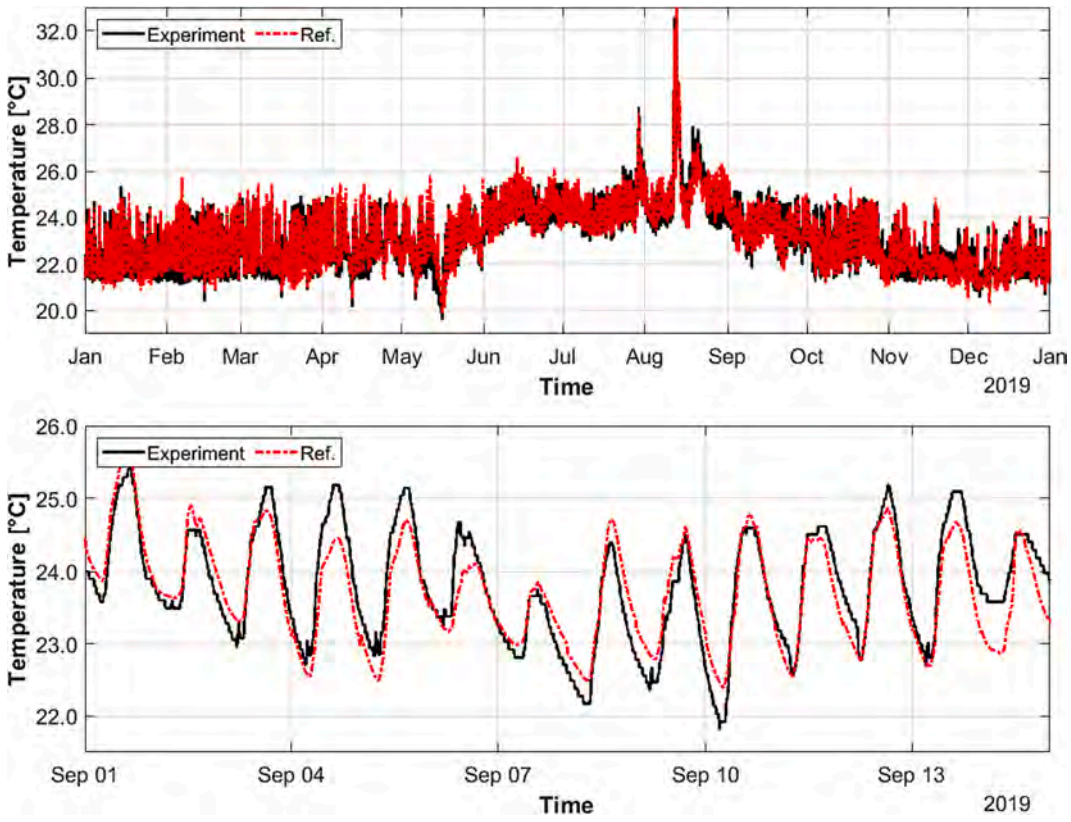

Fig. 14. Yearly profiles (top) of temperature in the building zone and zoom on two weeks (bottom): comparison of measured (labelled Experiment) and forecasted with *3R3C* model (labelled Ref.).

time step, is better centred than the *4R2C-fv* variant and achieves a smaller MAE of 0.46 °C instead of 0.52 °C for the *4R2C-fv* model. Nevertheless, the *4R2C-fd* model has much more outliers, which could be explained by the necessary smaller time step. It also requires over three times longer runtime. The variants *4R2C-fv-na* with the *coupling to the zone below* performs even worse than *4R2C-fv*, with 0.7 °C MAE.

In comparison, the simpler *3R3C* and *4R4C* models achieve 0.25 °C MAE. The simplicity of *3R3C* and *4R4C* models, allowing a fully data-driven parameter identification, reveals to be a strength. Indeed, the 4R2C-*fd* and 4R2C-*fd* require assumptions based on manufacturer or field data. The *3R3C* model gives results of a slightly lower quality (1 % higher MAE) than the *4R4C* model, but the runtime is over four times shorter. This is expected thanks to the simpler structure of the *3R3C* model, with less parameters to be identified.

5.2.5. *Discussion of the façade model*

The box plots in Fig. 12 shows that the *enhanced* façade model slightly narrows the error bars. There are also less outliers, especially on the negative error side. This slight improvement is also visible on the histograms in Fig. 13, showing the relative frequency distribution for the two best state-space models –*3R3C and 4R4C*– with either the *enhanced* or the *simple* façade model. The 3R3C model with *enhanced* façade model achieves 0.25 °C MAE, 9 % lower than with the *simple* façade model. All variants show similar behaviour, with slightly better results with the

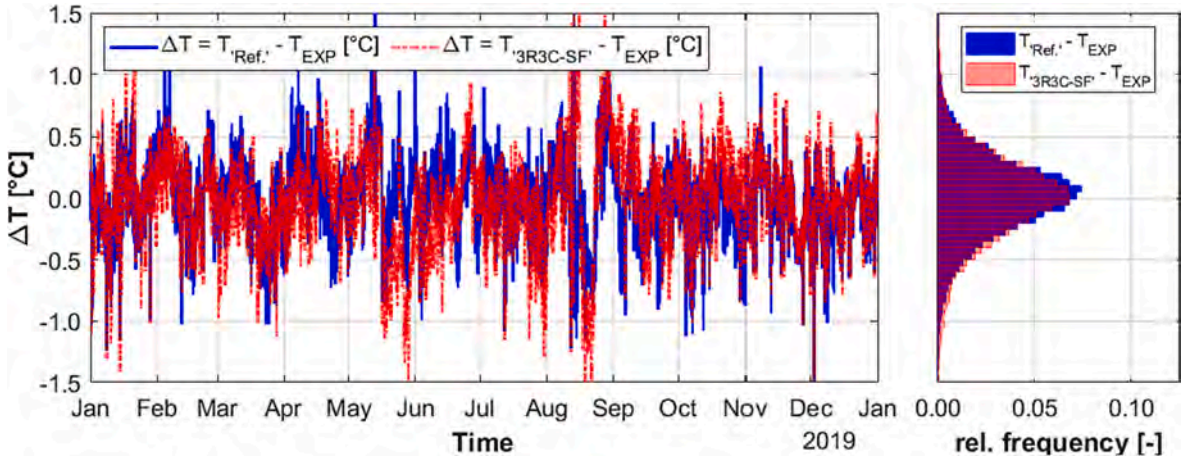

Fig. 15. Comparison of enhanced and simple façade models: Temperature deviation of the 24-hour forecast and the corresponding experimental data (subscript EXP) of the model 3R3C-EF (Ref.) and the model 3R3C-SF.

enhanced façade model than with the *simple* façade model. Worth noticing is that the similar runtime (6 % is no significant deviation) is explained by the fact that in operation both façade models are equally heavy. Indeed, the additional calculations for the *enhanced* façade model need to be run only once and have been run prior to this yearly simulation.

In Fig. 15, the temperature deviation between the 24-hour forecast of the model '3R3C-EF' (='Ref.') –with enhanced façade model– and the 24-hour forecast of model '3R3C-SF' –with simple façade model– is shown. The deviation is statistically very similar and no seasonal pattern can be distinguished for one or the other model. The enhanced façade improves the percentage of deviations under 0.5 °C by two points, reaching 88 %, instead of 86 % with the simple facade. Fig. 16 draws the deviation of these two models relative to each other. The difference is statistically centred and in 93 % of the cases below 0.5 °C. It does not reveal a clear seasonal influence either. An extra analysis of the model relative error depending on the weather conditions (temperature, solar irradiance) did not show any correlation. This suggests that the relative error between the façade model variants is not directly linked to the weather.

5.2.6. Stability of model parameters of 3R3C and 4R4C models with simple and enhanced façade models

The frequency distribution of the identified parameters –over a year of daily simulations– is presented in Fig. 17 for 3R3C and in Fig. 18 for 4R4C variants. The plots show for these two variants the results with both versions of the façade model: simple and enhanced.

A first observation is that *UA*, *gA* and C_{air} are the most stable in terms of order of magnitude, through time and for any variant. The only parameters that vary significantly are the *h* and *C* couples, linked to the heating and cooling systems: *FBH*, *DE* and *TABS*. The *ADI* parameters (h_{ADI} and C_{ADI}) show stronger variations in the 4R4C case than in the 3R3C case. This is a noteworthy difference, which enables a better understanding of the differences between both model structures, already mentioned in section 3.2). The 3R3C model has a single couple (*TABS*: h_{TABS} and C_{TABS}) for the heating and cooling elements. The remaining thermal mass of the building is fully represented by the *ADI* couple of parameters. This is different in the 4R4C variants, where two couples and are used for heating (*FBH*) and cooling (*DE*). Apart from free-running periods, one couple is used actively (e.g. *FBH* during heating), while the other couple is "inactive" (e.g. *DE* during heating). The "inactive" couple is then playing a similar role than *ADI*. The model has too many degrees of freedom. During free-running periods, the situation is even worse, with three parameters playing similar roles. These ill-posed configurations result in difficulties to converge. This is reflected in the triple runtime of 4R4C compared to 3R3C, as mentioned in section 5.2.4) iv (see values in Table 5).

To deepen the analysis, the timeline of the model parameters for every day of the year are shown in Fig. 19 for the reference model (3R3C-EF). The heating and cooling loads are plot in a second diagram below. This helps visualise a possible influence of the operation mode –heating, cooling or free-running– on the parameter values. No clear seasonal differences in the parameter values are revealed. The strong variations do not allow for direct physical interpretation of the values. Fig. 19 contributes to the awareness, that the analysis of a single parameter is also not meaningful: all the parameters build the model together with a certain interdependence. The timeline analysis shows that when a *h* parameter changes of order of magnitude, the associated *C* parameter also changes its order of magnitude. During some periods when a parameter is evaluated to its minimum boundary, variations of the associated parameter are observed, keeping the balance. For example, C_{TABS} often lies at its lower boundary (over 1/4 of the cases). Lowering this boundary has been tested, without benefit, as the lower capacitance value is compensated by the relative order of magnitude of the resistance. The lower boundaries set to zero look "infinitely" low in the logarithmic plot. The resistance parameters *h* indeed move close to zero in some cases. It would be an option to test a positive lower boundary for these parameters. It is unclear though, if the effect would be positive or not.

In the end, the changes in the order of magnitude of some parameters are not detectable in the model error timelines. The analysis of the parameters confirms the feasibility of the 3R3C model structure and its advantages compared to the 4R4C structure. The variability of the heating and cooling parameters proves to be acceptable, as no effect is reflected in the model performance.

6. Conclusion and perspective of the state space model development

The parameter studies shows that 15 min time step is short enough to capture fully the thermal dynamics of the building. Although 7 days start-up phase already gives good results, 14 days start-up phase are recommended, improving by 5 % the MAE for in the order of 14 % longer runtime. Training times of 14 to 28 days perform equally well. The longer training time of 28 days is selected in this study, which costs 50 % additional runtime compared to 14 days. The default least-square non linear algorithm (lsqnonlin) proved more stable than the tested alternative. The finer convergence criteria is used in the study, as it avoids days with degraded model quality in some variants. The coarser convergence criteria achieves almost the same results quality for the reference variant. It can also be considered to optimise the computing efforts (over 40 % runtime reduction). The default initial values for the

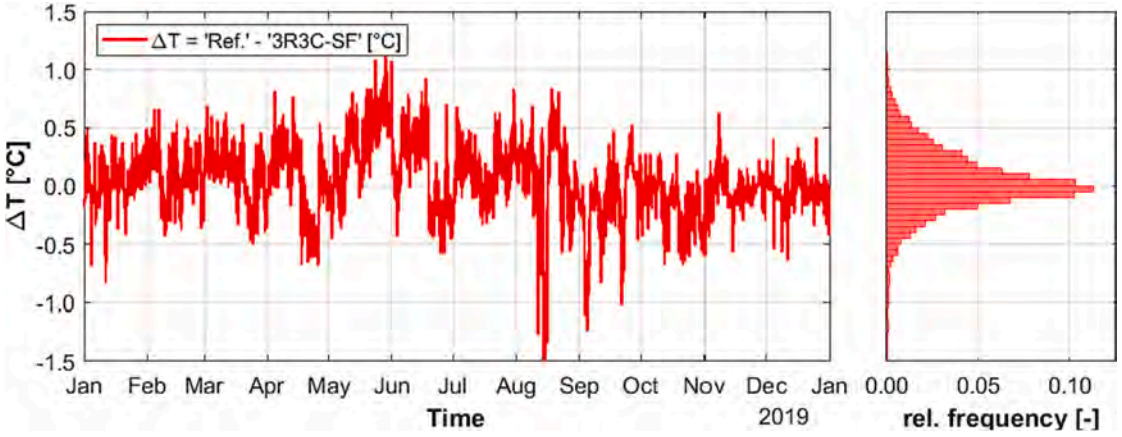

Fig. 16. Comparison of enhanced and simple façade models: Temperature deviation between the 24-hour forecast of the model 3R3C-EF (Ref.) and the model 3R3C-SF.

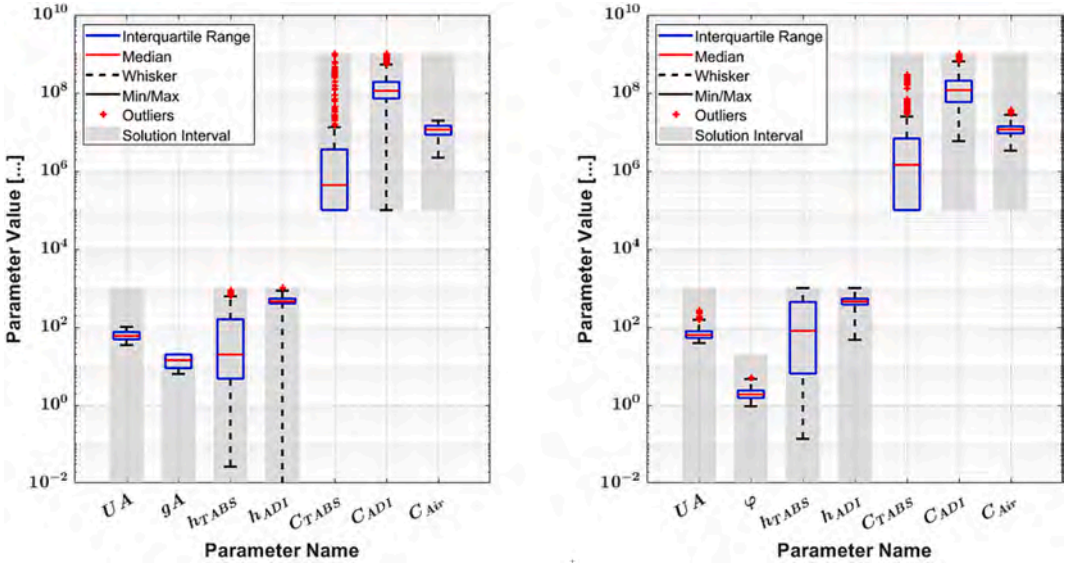

Fig. 17. Frequency distribution of the identified parameters for model 3R3C, with simple façade model (left) and enhanced façade model (right).

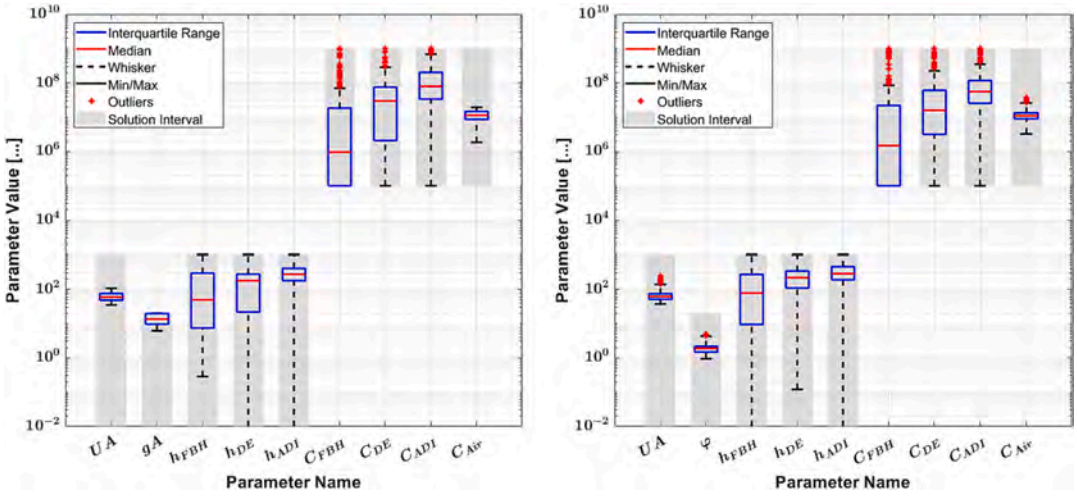

Fig. 18. Frequency distribution of the identified parameters for model 4R4C, with simple façade model (left) and enhanced façade model (right).

parameters are satisfying. Any combined modifications of these technical parameters should be tested to draw conclusions, as the effect of a single parameter modification cannot be extrapolated. Regarding the regular parameter update, the influence of the time of day (other than midnight) and of the frequency (other than daily, for example hourly or every couple of days) on the model performance could be investigated.

The results analysis of the physical model variants led to the selection of the *3R3C model* with the *enhanced façade model*. It achieves 0.25 °C of MAE over a year of simulation. The *4R4C* variant is modelling separately the ceiling cooling and floor heating. It provides slightly better results with just 1 % lower MAE than *3R3C* variant, but requires over three times longer runtime. Therefore the *3R3C* model is preferred. Unexpectedly, the models with the *finite difference method* (*4R2C-fd*) and with the *finite volume method* (*4R2C-fv*) provide worse results than the 3R3C and 4R4C models. The finer modelling of the heating and cooling slabs does not bring any advantage.

The *3R3C* variant with the *simple façade model* performs almost as well (0.27 °C MAE). This result shows that the *simple façade model* can be used in specific cases, even with complex glass facades. In the present study, thanks to a precise slat angle control, no direct sunlight is transmitted through the slats. In this specific case, the simple façade model proves valid. In the general case of shutters with movable slats, the enhanced façade model is expected to perform better. Remarkably, the enhanced façade model only requires additional pre-processing: in operation, it is running as fast as the simple one. Nevertheless, the characteristic map behind the *enhanced façade model* requires information on the facade for a detailed window model with external shading model. Even without developing an entire white-box model, this requires additional setup effort. The advantage of the conventional state-space model, with the simple façade model, is that less information on the building is required, enabling a fully data-driven parameter identification. Therefore the conclusion that the *3R3C* state-space model with the *enhanced façade model* when possible, can be used with confidence to operate a predictive control system.

Based on this single zone model, it is intended to replicate the model to all the zones of the building under study. In this way, the entire building will be modelled. This will enable the implementation of a Model Predictive Control (MPC) for the entire building. The short training data requirement makes the proposed grey-box model well suited for an MPC. To set the training period duration, the duration of free-running operation should be kept in mind, when using the 3R3C model, because of the combined parameters for heating and cooling. The

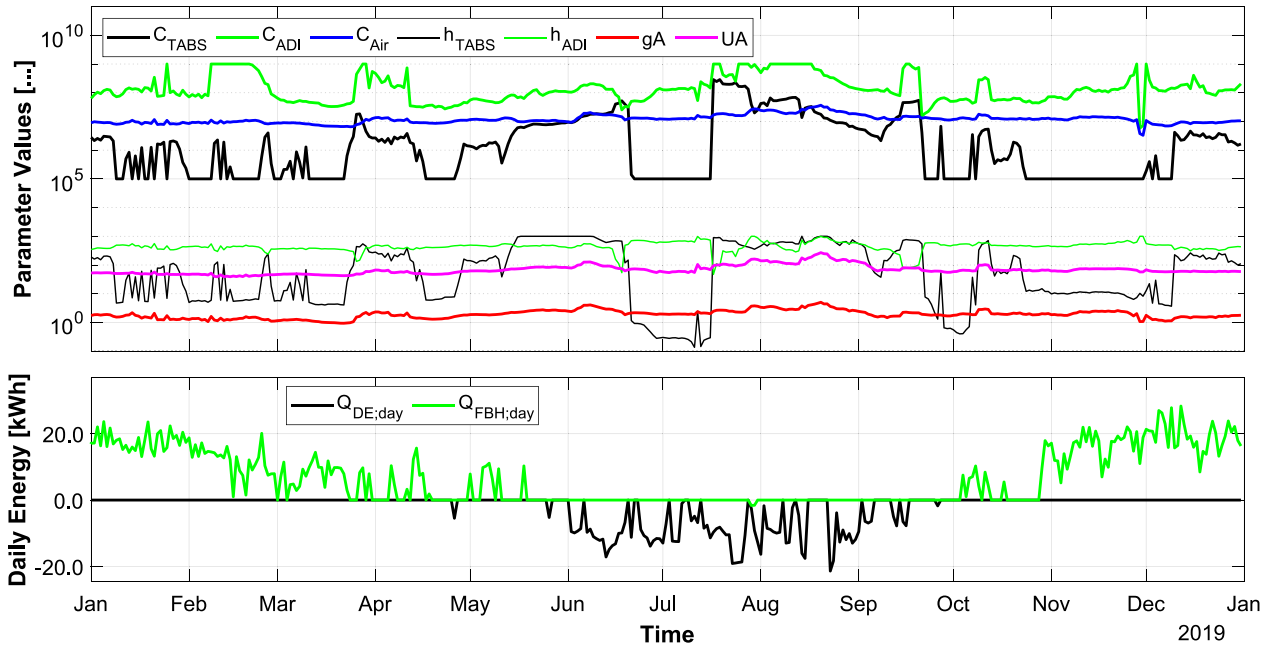

Fig. 19. Timeline of parameters of the 3R3C-EF model for every day of the year of demonstration (top). Daily energy consumption for heating (positive values) or cooling (negative values) (bottom).

reduced order of the 3R3C model should facilitate the formulation of an optimisation problem with Mixed Integer Linear Programming (MILP).

The proposed model performs well in a building with a complex configuration. For application in other buildings, the optimal technical parameters might be adjusted according to the thermal inertia of the construction. The building under study has low thermal mass in the façade, but concrete slabs in floors and roof, which provide thermal inertia. In buildings with higher thermal inertia, the 15 min time step can be used, but the startup and training phases might need to be longer, to adapt to slower thermal dynamics. The thermal dynamics should be well captured in buildings with less thermal inertia, as long as the time constant remains significantly longer than the time step duration. For solid facades with a higher thermal inertia than a glass façade, special attention might be required to validate or adjust the model structure. The model is expected to be useful for other buildings having a share of glass façade, especially to deal with external shading system. The model should work similarly in office buildings and residential buildings. The proposed approach is expected to be suitable for other buildings with TABS, in particular in combination with an Air Handling Unit. The monitoring requirements for the proposed approach include typical measurement data (temperature, power meter), as well as heat meters for the TABS and air flow meter for the AHU. When this data is available, the model can be transferred to other buildings.

Declaration of Competing Interest

The authors declare that they have no known competing financial interests or personal relationships that could have appeared to influence the work reported in this paper.

Acknowledgments

The work presented is based on research conducted within the framework of the project Prescient building Operation utilizing Real Time data for Energy Dynamic Optimization (PRELUDE): https://prelude-project.eu/. This project has received funding from the European Union's Horizon 2020 research and innovation programme under Grant Agreement N° 958345 (Call identifier: LC-EEB-07-2020).

References

[1] World Energy Outlook, International Energy Agency (IEA) (2021) 386. https://www.iea.org/reports/world-energy-outlook-2021.
[2] A. Afram, F. Janabi-Sharifi, Theory and applications of HVAC control systems – a review of model predictive control (MPC), Build. Environ. 72 (2014) 343–355, https://doi.org/10.1016/j.buildenv.2013.11.016.
[3] G. Serale, M. Fiorentini, A. Capozzoli, D. Bernardini, A. Bemporad, Model Predictive Control (MPC) for enhancing building and HVAC system energy efficiency: problem formulation, applications and opportunities, Energies 11 (2018) 631, https://doi.org/10.3390/en11030631.
[4] J. Drgoňa, J. Arroyo, I. Cupeiro Figueroa, D. Blum, K. Arendt, D. Kim, E.P. Ollé, J. Oravec, M. Wetter, D.L. Vrabie, L. Helsen, All you need to know about model predictive control for buildings, Annu. Rev. Control. 50 (2020) 190–232, https://doi.org/10.1016/j.arcontrol.2020.09.001.
[5] A. Arteconi, D. Costola, P. Hoes, J.L.M. Hensen, Building Performance, Analysis of control strategies for thermally activated building systems under demand side management mechanisms, Energ. Buildings 80 (2014) 384–393, https://doi.org/10.1016/j.enbuild.2014.05.053.
[6] J. Romaní, A. de Gracia, L.F. Cabeza, Simulation and control of thermally activated building systems (TABS), Energ. Buildings 127 (2016) 22–42, https://doi.org/10.1016/j.enbuild.2016.05.057.
[7] M. Sourbron, C. Verhelst, L. Helsen, Building models for model predictive control of office buildings with concrete core activation, J. Build. Perform. Simul. 6 (2013) 175–198, https://doi.org/10.1080/19401493.2012.680497.
[8] H. Viot, A. Sempey, L. Mora, J.C. Batsale, J. Malvestio, Model predictive control of a thermally activated building system to improve energy management of an experimental building: Part II - Potential of predictive strategy, Energ. Buildings 172 (2018) 385–396, https://doi.org/10.1016/j.enbuild.2018.04.062.
[9] J.(. Feng, F. Chuang, F. Borrelli, F. Bauman, Model predictive control of radiant slab systems with evaporative cooling sources, Energ. Buildings 87 (2015) 199–210.
[10] Y. Chen, M. Guo, Z. Chen, Z. Chen, Y. Ji, Physical energy and data-driven models in building energy prediction: a review, Energy Rep. 8 (2022) 2656–2671, https://doi.org/10.1016/j.egyr.2022.01.162.
[11] K. Arendt, M. Jradi, H.R. Shaker, C.T. Veje, Comparative analysis of white-, gray- and black-box models for thermal simulation of indoor environment: teaching building case study, (2018).
[12] M. Rätz, A.P. Javadi, M. Baranski, K. Finkbeiner, D. Müller, Automated data-driven modeling of building energy systems via machine learning algorithms, Energ. Buildings 202 (2019), 109384, https://doi.org/10.1016/j.enbuild.2019.109384.
[13] Y. Li, Z. O'Neill, L. Zhang, J. Chen, P. Im, J. DeGraw, Grey-box modeling and application for building energy simulations - A critical review, Renew. Sustain. Energy Rev. 146 (2021), 111174, https://doi.org/10.1016/j.rser.2021.111174.
[14] J. Arroyo, F. Spiessens, L. Helsen, Identification of multi-zone grey-box building models for use in model predictive control, J. Build. Perform. Simul. 13 (2020) 472–486, https://doi.org/10.1080/19401493.2020.1770861.
[15] A. Afram, F. Janabi-Sharifi, Gray-box modeling and validation of residential HVAC system for control system design, Appl. Energy 137 (2015) 134–150, https://doi.org/10.1016/j.apenergy.2014.10.026.

[16] A. Fonti, G. Comodi, S. Pizzuti, A. Arteconi, L. Helsen, Low order grey-box models for short-term thermal behavior prediction in buildings, Energy Procedia 105 (2017) 2107–2112, https://doi.org/10.1016/j.egypro.2017.03.592.
[17] G. Reynders, J. Diriken, D. Saelens, Impact of the heat emission system on the identification of grey-box models for residential, Buildings 78 (2015) 3300–3305.
[18] B. Cui, C. Fan, J. Munk, N. Mao, F. Xiao, J. Dong, T. Kuruganti, A hybrid building thermal modeling approach for predicting temperatures in typical, detached, two-story houses, Appl. Energy 236 (2019) 101–116, https://doi.org/10.1016/j.apenergy.2018.11.077.
[19] M.H. Shamsi, W. O'Grady, U. Ali, J. O'Donnell, A generalization approach for reduced order modelling of commercial buildings, Energy Procedia 122 (2017) 901–906, https://doi.org/10.1016/j.egypro.2017.07.401.
[20] M.H. Shamsi, U. Ali, E. Mangina, J. O'Donnell, Feature assessment frameworks to evaluate reduced-order grey-box building energy models, Appl. Energy 298 (2021), 117174, https://doi.org/10.1016/j.apenergy.2021.117174.
[21] R. De Coninck, Grey-Box Based Optimal Control for Thermal Systems in Buildings – Unlocking Energy Efficiency and Flexibility, 2015. https://doi.org/10.13140/RG.2.1.4761.6166.
[22] R. De Coninck, F. Magnusson, J. Åkesson, L. Helsen, Toolbox for development and validation of grey-box building models for forecasting and control, J. Build. Perform. Simul. 9 (3) (2016) 288–303.
[23] S. Freund, G. Schmitz, Development of a Framework for Model Predictive Control (MPC) in a Large-Sized Office Building Using Modelica Grey-Box Models, 2019. https://doi.org/10.26868/25222708.2019.210443.
[24] R. De Coninck, F. Magnusson, J. kesson, L. Helsen, Grey-Box Building Models for Model Order Reduction and Control, 2014. https://doi.org/10.3384/ECP14096657.
[25] S. Freund, G. Schmitz, C. Tiemann, Adaptive Grey-Box Models for Model Predictive Building Control Using the Unscented Kalman Filter, 2021.
[26] S. Rouchier, M. Rabouille, P. Oberlé, Calibration of simplified building energy models for parameter estimation and forecasting: Stochastic versus deterministic modelling, Build. Environ. 134 (2018) 181–190, https://doi.org/10.1016/j.buildenv.2018.02.043.
[27] A.R. Coffman, P. Barooah, Simultaneous identification of dynamic model and occupant-induced disturbance for commercial buildings, Build. Environ. 128 (2018) 153–160, https://doi.org/10.1016/j.buildenv.2017.10.020.
[28] D. Kim, J. Cai, K.B. Ariyur, J.E. Braun, System identification for building thermal systems under the presence of unmeasured disturbances in closed loop operation: Lumped disturbance modeling approach, Build. Environ. 107 (2016) 169–180, https://doi.org/10.1016/j.buildenv.2016.07.007.
[29] M.J. Ellis, Machine Learning Enhanced Grey-Box Modeling for Building Thermal Modeling, in: 2021 American Control Conference (ACC), 2021: pp. 3927–3932. https://doi.org/10.23919/ACC50511.2021.9482715.
[30] T. Péan, S. Ibañez Iralde, J. Pascual, J. Salom, Design and test of reduced grey-box models adapted to office buildings, in: 2021. https://doi.org/10.26868/25222708.2021.30512.
[31] H. Viot, A. Sempey, L. Mora, J.C. Batsale, J. Malvestio, Model predictive control of a thermally activated building system to improve energy management of an experimental building: Part I—Modeling and measurements, Energ. Buildings 172 (2018) 94–103, https://doi.org/10.1016/j.enbuild.2018.04.055.
[32] D. Picard, M. Sourbron, F. Jorissen, J. Cigler, Z. Vá?a, L. Ferkl, L. Helsen, Comparison of Model Predictive Control performance using grey-box and white box controller models, International High Performance Buildings Conference. (2016). https://docs.lib.purdue.edu/ihpbc/203.
[33] B. Huchuk, H.B. Gunay, W. O'Brien, C.A. Cruickshank, Model-based predictive control of office window shades, Build. Res. Inf. 44 (2016) 445–455, https://doi.org/10.1080/09613218.2016.1101949.
[34] J. Xie, A. Sawyer, Machine Learning-Based Model Predictive Control for Automated Shading Systems, 2021.
[35] P. Klanatsky, F. Veynandt, R. Stelzer, C. Heschl, Monitoring dataset from an office room in a real operating building, suitable for state-space energy modelling, Dataset or Other Products (Fh-Burgenland.At). (2023). https://doi.org/10.57739/3727.
[36] IDA ICE - Simulation Software | EQUA, (n.d.). https://www.equa.se/en/ida-ice (accessed July 12, 2022).
[37] F. Veynandt, C. Heschl, Modeling of solar radiation transmission through triple glazing based only on on-site measurements, in: Verlag der Technischen Universität Graz, Online Conference, 2020. https://doi.org/10.3217/978-3-85125-786-1-03.
[38] F. Veynandt, C. Heschl, P. Klanatsky, H. Plank, Complex glass facade modelling for Model Predictive Control of thermal loads: impact of the solar load identification on the state-space model accuracy, Leykam, 2020. http://hdl.handle.net/20.500.11790/1396 (accessed January 31, 2022).
[39] J. Durbin, S. Koopman, Time Series Analysis by State Space Methods, OUP Catalogue. (2001). https://www.semanticscholar.org/paper/Time-Series-Analysis-by-State-Space-Methods-Durbin-Koopman/8fd8e974c243267057372cfa867568d05afff494 (accessed December 20, 2022).
[40] T.O. Hodson, Root-mean-square error (RMSE) or mean absolute error (MAE): when to use them or not, Geosci. Model Dev. 15 (2022) 5481–5487, https://doi.org/10.5194/gmd-15-5481-2022.